

NASA Technical Memorandum 78793

**POWERED LOW-ASPECT-RATIO WING IN GROUND
EFFECT (WIG) AERODYNAMIC CHARACTERISTICS**

**James L. Thomas, John W. Paulson, Jr. and
Richard J. Margason**

**(NASA-TM-78793) POWERED LOW-ASPECT-RATIO
WING IN GROUND EFFECT (WIG) AERODYNAMIC
CHARACTERISTICS (NASA) 49 p HC A03/MF A01**

N79-31141

CSSL 01A

Unclas

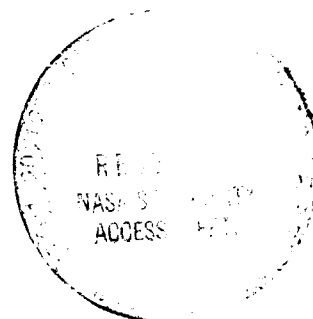
G3/02 35702

July 1979

NASA

National Aeronautics and
Space Administration

Langley Research Center
Hampton, Virginia 23665



SUMMARY

An investigation of a wing-in-ground effect configuration has been conducted in the Langley V/STOL tunnel as a joint effort between the David W. Taylor Naval Ship Research and Development Center and the National Aeronautics and Space Administration. The present configuration used large diameter, low-pressure-ratio fans mounted about 0.76 wing chord ahead of the wing leading edge to achieve a power-augmented ram wing during operation in-ground effect. The investigation included tests to determine both in- and out-of-ground effect aerodynamic transition characteristics from very low speeds to cruise speeds.

Results from the investigation dealt primarily with determination of the aerodynamic/propulsive performance interaction. Both boundary-layer control on the wing and nacelle power increased the lift in- and out-of-ground effect. This power-augmented lift is required for low-speed flight. Flap deflection and/or thrust coefficient variations provided the best method for flight-path control. Increasing flap deflection reduced the in-ground effect lift benefit, especially when the flap deflection protruded below the lower surface of the wing endplates. The nacelle deflection primarily affected the pitching moment through both direct thrust and aerodynamic interference increments. High nacelle deflections were useful in reducing the pitching-moment trim requirement for the vehicle particularly at the high thrust coefficients. There was a thrust loss when the efflux is trapped under the wing which reduced the effective thrust to weight available for acceleration by about a third of the installed thrust-to-weight ratio.

INTRODUCTION

During the last 25 years, many types of aircraft configurations have been studied in the development of short takeoff and landing (STOL) performance capability. This work has involved considerable research in high-lift devices and propulsive high-lift aerodynamics, where the propulsion system efflux is directed onto wing high-lift devices to provide lift augmentation. One unconventional aircraft configuration is considered in the present paper.

An investigation of a wing-in-ground effect configuration has been conducted in the Langley V/STOL tunnel as a joint effort between the David W. Taylor Naval Ship Research and Development

Center and the National Aeronautics and Space Administration. This vehicle has the propulsion system located well forward on the fuselage so that the jet efflux can be directed either over or under a low-aspect-ratio wing. Unlike conventional externally blown flaps, which provide lift by turning the jet efflux, the present system provides lift near the ground by using an air cushion under the wing. The lift can be controlled by the deflection of the jet efflux as well as by the deflection of the wing flap. A very significant lift increase is developed in hover. As forward speed increases, the operating mode is similar to a ram wing, that is, very much like a ground-effect machine. This concept is called the augmented ram wing.

This concept has been studied at the Langley Research Center during the past 8 years. A configuration (fig. 1) investigated in the early 70's in the V/STOL tunnel (refs. 1 to 3) used an aspect-ratio-2 wing with triangular-shaped endplates and high-pressure-ratio jet engines mounted on nacelles located ahead of the wing. These investigations included both results from static hover conditions (ref. 1) and results from low subsonic speeds through the transition regime, including both in-ground effect and out-of-ground effect conditions (refs. 2 and 3). The configuration shown in figure 2 has a similar engine-wing configuration and has been tested in the 12-foot tunnel at Langley. Results from those tests showed some fairly significant lift increases in ground effect.

The present investigation deals with a configuration which uses low-pressure-ratio fans mounted ahead of the wing and is based on the concepts of Gallington (refs. 4 to 6) which achieve very efficient air-cushion support. The present tests were conducted in the Langley V/STOL tunnel and included both in- and out-of-ground effect aerodynamic transition characteristics from very low speeds to cruise speeds. The tests included a configuration buildup from the basic wing-fuselage to the vehicle with powered nacelles. Results are presented in three parts: (1) the out-of-ground effect aerodynamics; (2) the in-ground effect aerodynamics; and (3) a brief analysis of takeoff and landing characteristics.

SYMBOLS

b	wing span, m (ft)
c	wing chord, m (ft)
C_D	drag coefficient
C_L	lift coefficient
$C_{L,\infty}$	lift coefficient out-of-ground effect

C_m	pitching-moment coefficient
$C_{m,0}$	pitching-moment coefficient at zero thrust coefficient
C_T	thrust coefficient
C_μ	boundary-layer-control momentum coefficient
h	height measured from the ground to the quarter chord in the wing chord plane, cm (ft)
L	lift, N (lbf)
L	lift out-of-ground effect, N (lbf)
P_{ref}	reference pressure for boundary-layer-control plenum, Pa (lbf/ft ²)
p_s	static pressure, Pa (lbf/ft ²)
p_t	total pressure, Pa (lbf/ft ²)
S	wing area, m (ft ²)
T	fan thrust, N (lbf)
V	velocity, m/sec (ft/sec)
W	weight, kg (lbm)
α	angle of attack, deg
δ_f	flap deflection, deg
δ_N	nacelle deflection, deg
γ	flight-path angle, deg

Subscripts:

b	moving belt
E	thrust removed
∞	free stream

Notation:

BLC	boundary-layer control
B.L.	butt line, cm

W.L. water line, cm
B.S. body station, cm

MODEL AND TESTS

A three-view sketch indicating the major geometric characteristics of the configuration is presented in figure 3. The wing has a 1-m (3.3-ft) chord and 2-m (6.6-ft) span and uses a Clark-Y airfoil section (12-percent thick). The fans have a 19-cm (7.48-in.) exit diameter and were located 4 exit diameters ahead of the wing leading edge. The nacelle mount had a large fairing which permitted changing the height of the nacelle with respect to the wing.

Details of the nacelle installation relative to the wing are shown in figure 4. The low-height nacelle centerline is about 16 percent of the chord above the lower surface of the wing, and the mid-height nacelle centerline is about 26 percent of the chord above the lower surface of the wing. The nacelles could be deflected from 0° to 40° , and the flap could be deflected from 0° to 60° . It should be noted that near the 20° flap deflection, the trailing edge of the flap coincided with the lower surface of the wing endplates, providing a trap on three sides for the air exhaust from the nacelle fans. When the flaps are deflected greater than 20° , their trailing edge projects below the bottom edge of the endplates which can result in a very large gap between the ground and the bottom of the endplates.

A photograph is presented in figure 5 of the model installed in the V/STOL tunnel in a low height configuration with the nacelles set at a moderate deflection angle. At the end of the fuselage, two angle irons were installed to support counterweights which statically balanced the weight of the model on the strain-gage balance.

The test section of the V/STOL tunnel has a height of 4.42 m (14.50 ft), a width of 6.63 m (21.75 ft), and a length of 14.24 m (50.00 ft). The model was sting mounted using a six-component strain-gage balance system which measured the forces and moments. The angle of attack was determined from an accelerometer mounted in the fuselage.

The tests were conducted at a free-stream dynamic pressure of 575 Pa (12 lbf/ft²) which corresponds to a velocity of 30.5 m/sec (100.0 ft/sec). The Reynolds number of these tests was approximately 2.1×10^6 based on the wing chord. The in-ground effect aerodynamic characteristics were obtained at 0° and 4° angle of attack through a height range of approximately 0.08 to 0.50 wing spans. Initial tests at low heights were conducted with a moving groundbelt system. Most of the tests were conducted, however, with the moving groundbelt stationary but with the boundary layer

removed through a perforated floor section at the front of the test section. Under these circumstances, a boundary layer develops between the trailing edge of the perforated plate and the station of the model. It is estimated that this boundary layer is relatively thin (5 cm (2 in.)). No corrections were applied to the data.

THRUST CALIBRATIONS

The total fan thrust was determined by summing the contributions from each of the four fans calibrated separately. The thrust from each of the individual fans is shown in figure 6 as a function of total pressure to static pressure ratio. The pressures are averages of 12 total pressure probes and 4 static pressures measured in the exit of each fan. It can be seen from the curves that the calibrations provide very similar linear variations of thrust with increase of pressure ratio. For the tests, the pressure ratio was monitored and used to determine the thrust.

The flap boundary-layer control (BLC) is provided through a slot located in the wing just ahead of the flap leading edge at the 70-percent chord location across the full span of the wing. The thrust from the BLC slot was calibrated as a function of a reference pressure measured in an internal pressure chamber. The calibration for this thrust is presented in figure 7. This thrust was nondimensionalized by the tunnel dynamic pressure and the wing area to provide a value for BLC momentum coefficient C_{μ} .

The BLC used during the tests was a fixed percent of the fan thrust which represents a constant bleed from the primary engines. The variation of BLC momentum coefficient as a function of thrust coefficient for this investigation is presented in figure 8. C_{μ} represents approximately 12 percent of the fan thrust coefficient C_T . The direction of C_{μ} tended to be tangent to the upper surface of the wing at the trailing edge.

RESULTS AND DISCUSSION

Out-of-Ground Effect Aerodynamic Characteristics

Wing-fuselage configuration.- The effect of flap deflection for the wing-fuselage configurations without BLC is presented in figure 9 for flap deflections of 0° , 10° , and 20° . The lift data show the expected variation of lift with angle of attack and show that maximum lift coefficient with 0° flap deflection is in the neighborhood of 1.0. There is an increase in lift coefficient of about 0.2 throughout the angle-of-attack range for the 10° flap deflection. A similar increment of lift coefficient is obtained from 10° to 20° flap deflection at 0° angle of attack, but a

gradual flow separation with increasing angle of attack results in a smaller increment of lift increase near stall. The pitching-moment coefficient data show the expected unstable variation with increase in lift and nose-down increment with increasing flap deflection.

The effect of flap deflection on the aerodynamic characteristics for the wing-fuselage configuration is presented in figure 7 for $C_{\mu} = 0.06$. The results are very similar to the previous data except that they do show: (1) an increase in lift throughout the angle-of-attack range for all flap deflections; (2) slightly larger nose-down moments; and (3) a drag polar that includes the thrust contribution from the BLC.

Complete configuration.- The power-off longitudinal aerodynamic characteristics are presented in figure 11 for the configuration with a 40° nacelle deflection and flap deflections of 0° , 20° , 40° , and 60° . These data show a large lift increase for the 20° flap deflection, a smaller lift increase for the 40° flap deflection, and a slight lift loss for the 60° flap deflection. These lift increments and increases in drag shown on the drag polar in figure 11 indicate the presence of flow separation at the higher flap deflections.

The results of the complete model configuration with powered nacelles and BLC are presented in figures 12 to 15. The longitudinal aerodynamic characteristics with 0° deflection for both the flap and nacelles are presented in figure 12. The expected variation of lift with angle of attack, pitching moment with lift, and lift-drag polars are shown. In this configuration, the lift-drag polars show an acceleration or climb capability for the range of thrust coefficients presented. The pitching-moment variation shows the expected nose-down variation with increase in thrust coefficient. Lift coefficients near 20° angle of attack for $C_T = 1.6$ are in the neighborhood of 2.5.

The longitudinal aerodynamic characteristics with 10° flap deflection and 19° nacelles deflection are presented in figure 13. Lift coefficients near 20° angle of attack for $C_T = 1.6$ are in the neighborhood of 3.5. The lift-drag polars show the strong acceleration capability for this configuration which would represent a configuration for takeoff and for climb. Pitching-moment coefficient variation with power off shows an unstable variation with lift and a pitching moment very near trim. As the power is applied, this unstable variation very rapidly becomes stable at a moderate angle of attack. At thrust coefficients of 1.1 and 1.6, this change from an unstable variation of pitch at the low angles of attack to a stable variation of pitch at moderate to high angles of attack is even more pronounced.

Results for this configuration with a flap deflection of 40° and a nacelle deflection of 19° are presented in figure 14. The

lift coefficient levels are not changed noticeably from the data in figure 13 with a 10° flap deflection. The lift-drag polars show a deceleration or descent capability through a wide range of lift coefficients.

Results for the configuration with a flap deflection of 40° and a nacelle deflection of 40° are presented in figure 15. The lift and drag characteristics are essentially unchanged from the previous figure with a 19° nacelle deflection. The most significant change is the pitching moment which is very near trim at this nacelle deflection. These data and those shown in figures 13 and 14 indicate that the flap provides an effective means for controlling flight-path angle, and the nacelle provides an effective means for trimming the configuration.

Figures 16 and 17 examine the effect of deflecting the fan thrust on the lift and pitching-moment characteristics. The data in figure 16 are for 0° angle of attack with the flaps deflected 20° and nacelle deflections of 14° , 19° , 24° , and 40° . The variation of lift coefficient as a function of thrust coefficient shows only a very small difference among the various nacelle deflections. The variation of total pitching-moment coefficient with thrust coefficients shows that increasing nacelle deflection provides an increment in nose-up moment throughout the thrust coefficient range.

Figure 17 presents the same data with the direct thrust contribution from the fans and the direct thrust from the BLC removed. The lift coefficient increase through the range of thrust coefficients represents the thrust-induced lift increment. The highest induced lift occurs with the lowest nacelle deflection, 14° ; a smaller lift induced increment occurs with the 19° and 24° nacelle deflections; and then only a modest induced lift increment exists for the 40° nacelle deflection. The thrust-removed pitching-moment coefficients show very similar curves for the three lower nacelle deflections. For the highest nacelle deflection, there is a larger nose-down variation of pitching moment with thrust coefficient.

In addition to removing the direct thrust, the pitching moment at zero thrust coefficient, $C_{m,0}$, are removed in figure 18 to show the variation of pitch increment due to induced aerodynamics for three flap deflections with nacelles deflected 19° and 40° . For the 19° nacelle deflection, there is a nose-down moment increment which increases with increased flap deflection. This indicates that the flow over the flap is attached so that additional lift is generated with increased flap deflection. When the nacelle is deflected 40° , the pitching-moment curves show variations at low C_T 's similar to those for the lower nacelle deflection. However, above a C_T of 0.8, the three curves tend toward the same slope and the same magnitude indicating that the the flow over the flap for all three deflections is separated. At the lower nacelle

deflection, the wing and flap are immersed in the efflux from the nacelles and the flow remains attached. However, at the higher nacelle deflections, the efflux passes below the wing and results in flow separation on the flap.

The preceding data were obtained with a low-height nacelle. The next two figures present results with the nacelle centerline mounted at the mid-height position. Figure 19 presents the effect of flap deflections of 0° , 10° , and 20° with a nacelle deflection of 26° and power off. The expected variations with increasing flap deflection are seen; a lift coefficient increase and a nose-down increase in pitching-moment coefficient.

Effects of thrust are presented in figure 20 for the 20° flap deflection with the 26° nacelle deflection. The expected increases in lift coefficient with angle of attack and the expected acceleration or climb capability are found. The pitching-moment coefficient variation with lift coefficient and thrust shows the same trends as for the low-height nacelle configuration.

Wing-In-Ground Effect Aerodynamic Characteristics

Effect of groundbelt test technique.- The results presented in figure 21 show the effect of the moving belt on the aerodynamic lift and drag coefficient as a function of height over span for the 20° flap and 24° nacelle deflection at an angle of attack of 0° . In all cases, the boundary-layer removal system was operating. On the curve of lift as a function of height over span, there is a shaded region in the upper left-hand corner. This represents the region determined by Turner (ref. 7) where the moving belt was needed to get a correct measurement of lift on a model.

The data presented in figure 21 include results with the moving belt stopped ($V_b/V_\infty = 0$) and with the moving belt on ($V_b/V_\infty = 1.0$). The lift coefficient data for the power-off condition show essentially no difference due to the belt; the two power-on curves show only a moderate difference at the lowest height for the 0.7 thrust coefficient. The variation of drag coefficient with height shows essentially no variation between belt on and belt off. Hence, for this model configuration and for the heights and lift coefficients involved in this investigation, the moving belt was not necessary for proper ground-effect simulation. Subsequent data in this report are presented without distinction for conditions with the belt and without the belt operating.

Wing-fuselage configuration.- The effect of flap deflection for the wing-fuselage configuration in-ground effect utilizing only BLC ($C_\mu = 0.06$) is presented at an angle of attack of 0° in figure 24. Variation of lift, drag, and pitching-moment coefficients are presented as a function of height over span. For all three flap deflections, there is a moderate increase in lift as the minimum ground height is reached. There is a small nose-down pitching

moment moment with decreasing height and very little change in drag coefficient with change in height.

Complete configuration.- Figures 23 to 26 present the effects of thrust through a ground height range for a range of flap and nacelle deflection angles. In all of the figures, the lift, drag, and pitching-moment coefficients are presented as a function of ground height. The data in figure 23 for a flap deflection of 10° and a nacelle deflection of 19° show that noticeable increases of lift coefficient are obtained with either decreasing height or increasing thrust coefficient. The variation of pitching moment shows an increase in nose-down increment at the minimum heights with increasing thrust coefficient. They also show that increases in thrust coefficient out-of-ground effect, or at the higher heights, provide a noticeable nose-up moment. Drag coefficient variations with height are almost nonexistent for this configuration.

In figure 24, data for a 20° flap deflection and a 19° nacelle deflection show similar increases in lift with reduction in height above the ground, nose-up moment increments out-of-ground effect with increasing thrust coefficient, and then nose-down variations in pitching moment as ground is approached. The drag coefficient shows very little effect of height except for a small increase at the lowest height for the highest thrust coefficient of 1.6.

When the flap deflection is increased to 40° with the 19° nacelle deflection unchanged (fig. 26), the lift coefficient no longer shows an increase with reduced ground height. In fact, there is a slight decrease. This is probably due to the fact that, for the 40° flap deflection, the trailing edge extended below the endplates of the wing. As the vehicle approached its minimum height, large gaps opened under the endplates between the ground and the bottom of the endplates. The efflux from the fans exhaust through these gaps so that the ability to trap an air cushion is essentially eliminated.

The pitching-moment data in figure 25 show a nose-up variation with height change. At the highest ground height, there is a nose-down pitching-moment variation with power. Both these trends are different from the lower flap deflection. Another difference is that the drag coefficient shows a reduction with reduced height. The progression of thrust recovery with change in thrust coefficient is quite different from the lower flap deflections indicating a significant lack of thrust recovery, particularly at the highest heights.

In figure 26, the nacelle deflection is increased to 40° . The lift and drag coefficient data are very similar to the results found in the previous figure. The biggest difference is that the pitching-moment data out-of-ground effect show a nose-up increment

with increasing thrust coefficient. The configuration is very near trim with relatively modest effects of heights.

The mid-height nacelle configuration in-ground effect using the 10° flap deflection and 26° nacelle deflection at an angle of attack of 6° is presented in figure 27. For the mid-height nacelle configuration, the expected increase in lift coefficient with reduced height is found; a moderate variation of drag coefficient with height is demonstrated; and the out-of-ground effect pitching moment shows an increment of nose-up moment with increasing thrust coefficient. There is a small nose-down variation of pitching moment with reduced ground height.

In summary, figure 28 presents the ratio of lift in-ground effect to lift out-of-ground effect through a range of heights for the configuration with a 19° low-height nacelle deflection and 0° angle of attack using a thrust coefficient of 0.7. The figure includes data for flap deflections of 10° , 20° , 40° , and 60° and shows the out-of-ground effect lift coefficient for each flap deflection. The largest lift gains are achieved with the 10° flap deflection; somewhat reduced lift gains are shown for the 20° flap deflection. For the 40° and 60° flap deflection, where the trailing edge protrudes below the bottom edge of the endplate, there is modest lift loss with reduced ground height.

TAKEOFF AND LANDING ANALYSIS

In an attempt to assess the aerodynamic characteristics presented in this report, an analysis was conducted of the takeoff and landing operation of a wing-in-ground effect vehicle. The purpose of this analysis is to determine the performance capabilities of such a vehicle. For purposes of analysis, the conceptual multimission power-augmented wing-in-ground effect vehicle presented in reference 8 was used. This configuration is a large vehicle with about 950,000 kg (2 million lb) gross weight and a high wing loading of about 9.58 Pa (200 lbf/ft²).

Takeoff Operation

The type of operation performed during a takeoff is illustrated in figure 29. The aircraft initially is floating on the water. With large flap and nozzle deflections, the nacelle efflux digs a hole in the water as demonstrated in previous water tank tests (ref. 9) and forms an air cushion under the wing. The vehicle then floats up on the air cushion. As the acceleration in-ground effect using the power-augmented ram is undertaken, both the flap and nacelle deflections are reduced. Once the vehicle achieves a cruise speed of approximately 171 knots, the flap and nacelle deflections are reduced to 0° for nonpower-augmented ram flight. It can then cruise either as a wing-in-ground effect, or it can cruise out-of-ground effect. For the analysis of takeoff and landing, the lift and drag coefficient data for the configuration

with 20° flap deflection and 19° nacelle deflection were utilized. It can be seen in figure 24 that variation of thrust coefficient provides control of acceleration, climb, or descent for the vehicle.

The results of the takeoff performance are presented in figure 30 using S.I. dimensions and in figure 31 using U.S. Customary dimensions. Figure 31 will be used for the purpose of discussion. Both figures present the wing loading for takeoff as a function of distance to transition to wingborne flight for ranges of thrust-to-weight ratio and thrust levels. The lift coefficient required for this transition is 1.8. Based on reference 6, the vehicle is assumed to have approximately 204 lbf/ft^2 wing loading, an overall weight of 2.09 million lb, and a thrust-to-weight ratio of 0.35 giving a thrust installed of 730,000 lb. This configuration is shown by the point on figure 31 and indicates a takeoff distance of approximately 6,700 ft can be achieved. In evaluating static calibration data, it was found that the forward thrust on the complete configuration was about two-thirds of the fan thrust. This result is due to trapping the efflux under the wing in the power-augmented ram and is probably a very real effect on the aircraft. Although there are no data herein at zero velocity (i.e., the start of takeoff run), this thrust loss was applied to the assumed installed thrust of 730,000 lb. Therefore, the initial thrust available was reduced to 489,000 lb. All other data used for calculating the takeoff performance are in figure 21. This thrust recovery factor is something that has been neglected to date in analyses of wing-in-ground effect performance and should be considered more closely in subsequent studies.

Landing Operation

In analyzing the landing configuration, it was determined that the data from the present investigation are only useful for the airborne portion of the landing. The deceleration achieved when the vehicle is on or near the water depends on the friction coefficient between the vehicle and the surface. This can be affected profoundly by dragging an object below the vehicle in the water, and a large range of friction coefficients can be achieved depending on the size of the sea anchor the vehicle uses.

The results presented in figure 32 for the S.I. units and in figure 33 for the U.S. Customary units deal only with the thrust required for approach and for waveoff. Figure 33 will be used for the purpose of discussion. In both cases, a lift coefficient of the order of 1.6 to 1.7 is considered. It is assumed that one quarter of the weight has been burned off in the form of fuel, so that the landing configuration has a wing loading of 150 lbf/ft^2 . For a 0.5° approach angle (solid lines), approximately 250,000 lb of thrust is needed and is indicated by the shaded region. For a waveoff condition, that is, a 1° climb rate, the dashed curves

indicate a slight increase in thrust required to 275,000 lb. Both thrust requirements are well under the 730,000 lb installed on the vehicle so this indicates there would be very little difficulty in achieving these types of approach or waveoff conditions.

CONCLUSIONS

An investigation of a wing-in-ground effect configuration utilizing large diameter nacelles located ahead of the wing leading edge has been conducted in the Langley STOL tunnel. These tests were conducted as a joint effort between the David W. Taylor Naval Ship Research and Development Center and the National Aeronautics and Space Administration. Results from the investigation indicate the following conclusions:

1. Both boundary-layer control and nacelle power increased the lift in- and out-of-ground effect, and this power-augmented lift is required for low-speed flight.

2. It was found that flap deflection and/or thrust coefficient variation provided the best methods for flight-path control. Increasing flap deflection reduces the in-ground effect lift benefit especially when the flap deflection protrudes below the lower surface of the wing endplates.

3. The nacelle deflection affects the pitching moment through the direct thrust and aerodynamic interference increments. High nacelle deflections are useful in reducing the pitching-moment trim requirement for the vehicle particularly at the high thrust coefficients. The nacelle deflection had little effect on lift coefficient.

4. It was found that the nacelle height makes very little difference in the overall aerodynamic characteristics.

5. There is a thrust loss when the efflux is trapped under the wing which reduces the effective thrust to weight available for acceleration by about a third of the installed thrust-to-weight ratio.

REFERENCES

1. Huffman, Jarrett K.; and Jackson, Charlie A., Jr.: Investigation of the Static Lift Capability of a Low-Aspect-Ratio Wing Operating in a Powered Ground-Effect Mode. NASA TM X-3031, 1974
2. Huffman, Jarrett K.; and Jackson, Charlie A., Jr.: Subsonic Investigation of Longitudinal and Lateral Aerodynamic Characteristics Of Unpowered Low-Aspect-Ratio Configuration With T-Tail. NASA TM X-3523, 1975
3. Gainer, Thomas G.; and Huffman, Jarrett K.: Longitudinal Characteristics of a Configuration With Exhaust From Forward-Mounted Engines Directed Over or Under the Wing to Produce High Lift. NASA TM X-3419, 1977
4. Gallington, Roger W.; and Chaplin, Harvey R.: Theory of Power Augmented Ram Lift at Zero Forward Speed. Aviation and Surface Effects Dept. Rept. ASED 350, Naval Ship Research and Development Center, Feb. 1976
5. Krause, Fred H.; and Gallington, Roger W.: Static Performance of a Power Augmented Ram Wing. Aviation and Surface Effects Dept. Rept. ASED-TM-16-76-76, D. T. Naval Ship Research and Development Center, May 1976
6. Rousseau, David G.; and Gallington, Roger W.: Performance Prediction Method for a Wing-in-Ground Effect Vehicle With Blowing Under the Wing. Aviation and Surface Effects Dept. Rep. ASED 379, D. T. Naval Ship Research and Development Center, March 1977
7. Turner, Thomas R.: Endless-Belt Technique for Ground Simulation. NASA SP-116, V/STOL and STOL Aircraft, April 1966, pp. 435-446
8. Papadales, Basil S., Jr.: The Performance of a Conceptual Multimission Power-Augmented-Ram Wing-in-Ground Effect Vehicle. Aviation and Surface Effects Dept. Rep. DTNSRDC ASED-395, D. W. Taylor Naval Ship Research and Development Center, September 1977
9. Krause, Fred H.: Evaluation of Power-Augmented-Ram Wing Operating Free in Heave and Pitch Over Water. Aviation and Surface Effects Dept. Rep. DTNSRDC ASED-385, D. T. Naval Ship Research and Development Center, August 1977

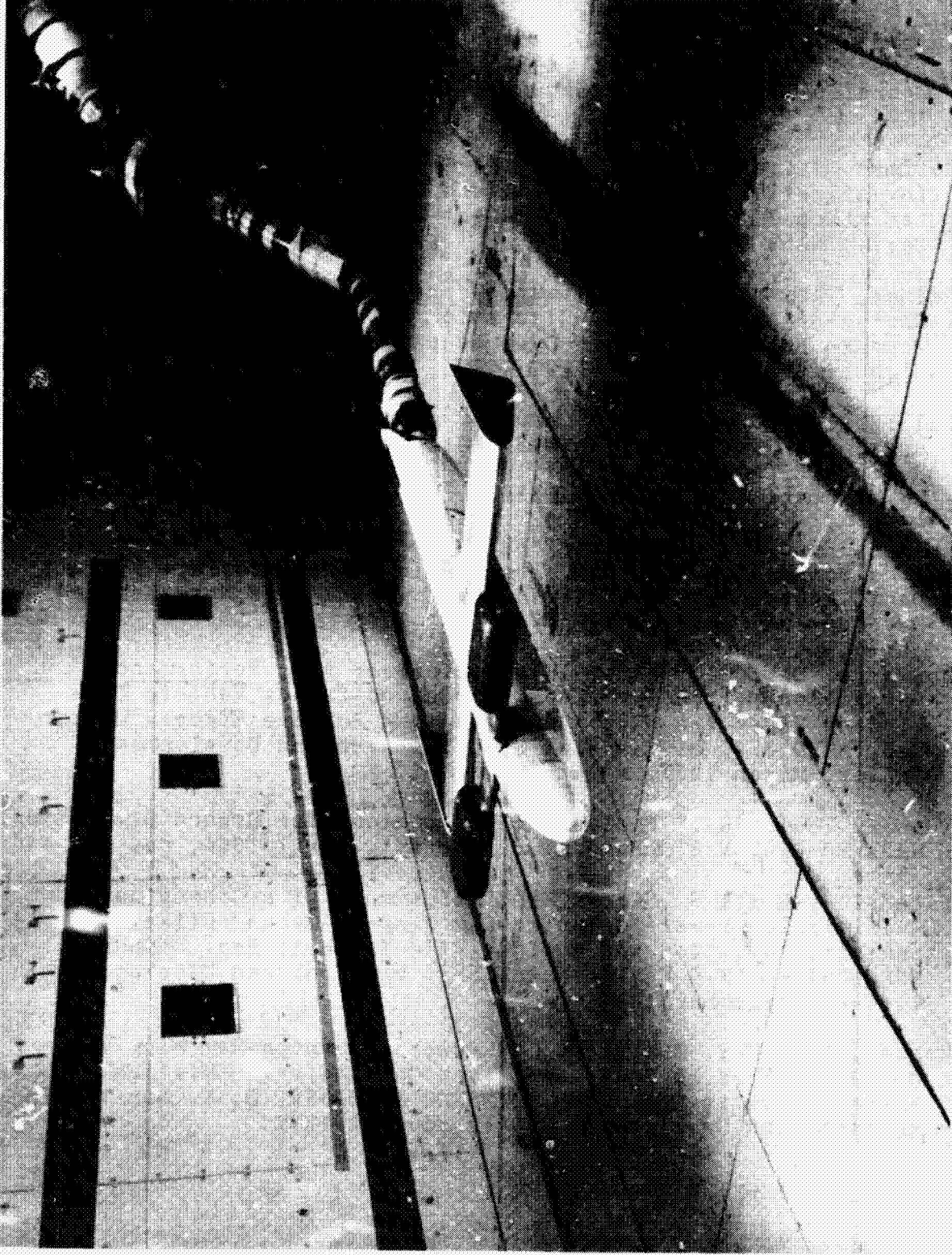


Figure 1.- First low-aspect-ratio wing in ground effect in Langley V/STOL tunnel.

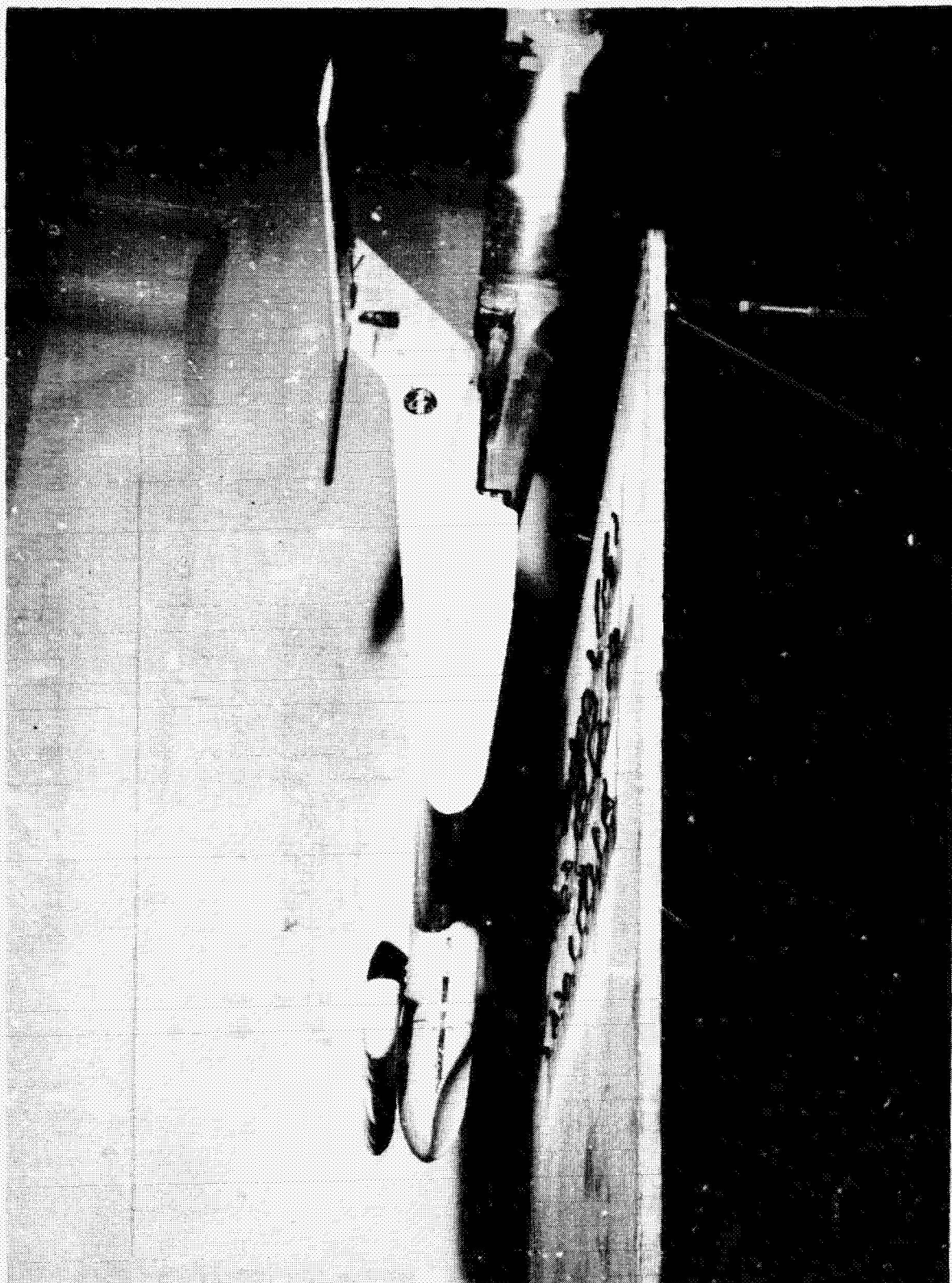


Figure 2.- Second low-aspect-ratio wing in ground effect in the Langley 12-foot tunnel.

ORIGINAL PAGE IS
OF POOR QUALITY

WING CHARACTERISTICS:

ASPECT RATIO 2.0
 SPAN 200 cm (78.74 in.)
 CHORD 100 cm (39.37 in.)
 CLARK Y AIRFOIL SECTION
 30% CHORD PLAIN FLAP
 WITH BLC

FAN CHARACTERISTICS:

EXIT DIAMETER 19.0 cm (7.5 in.)
 LENGTH 30.0 cm (11.8 in.)

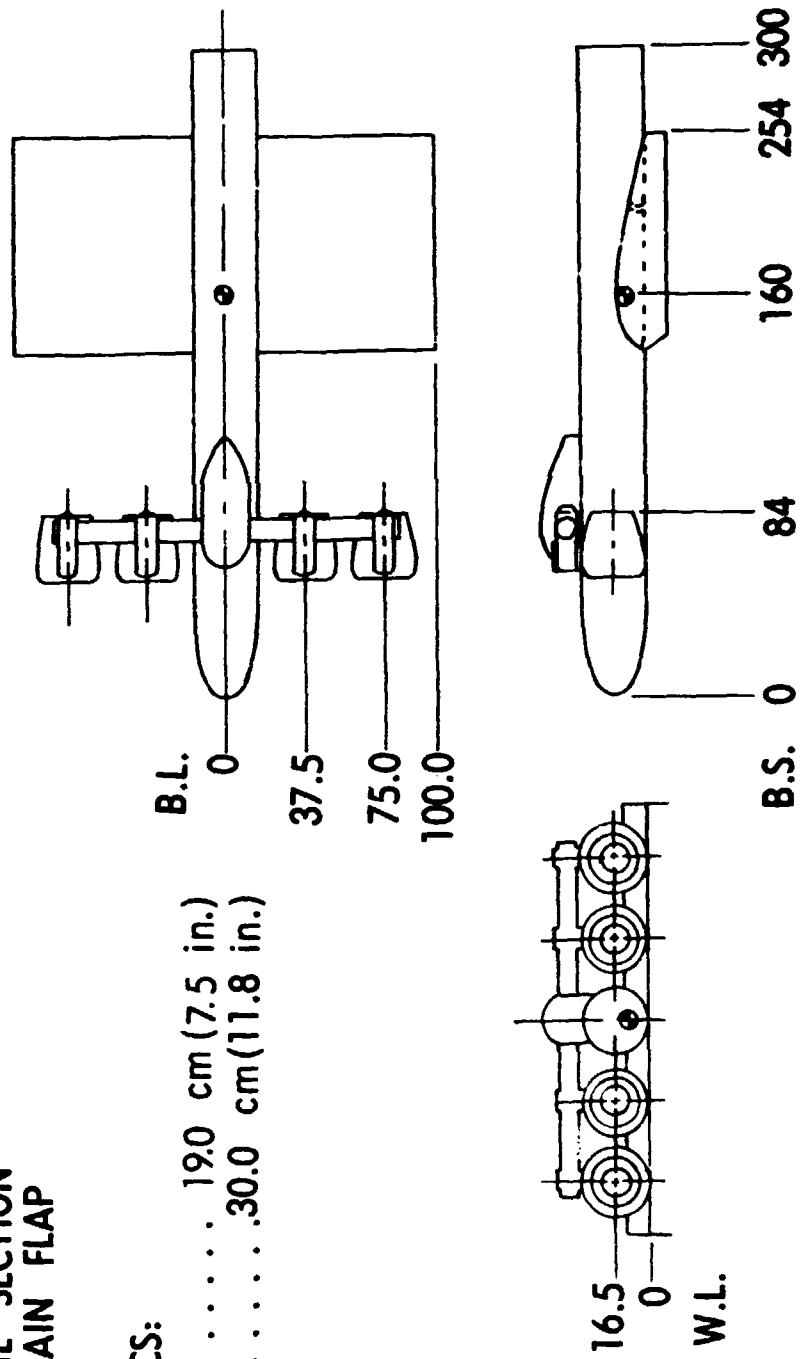


Figure 3.- Wing-in-ground effect (WIG) model.

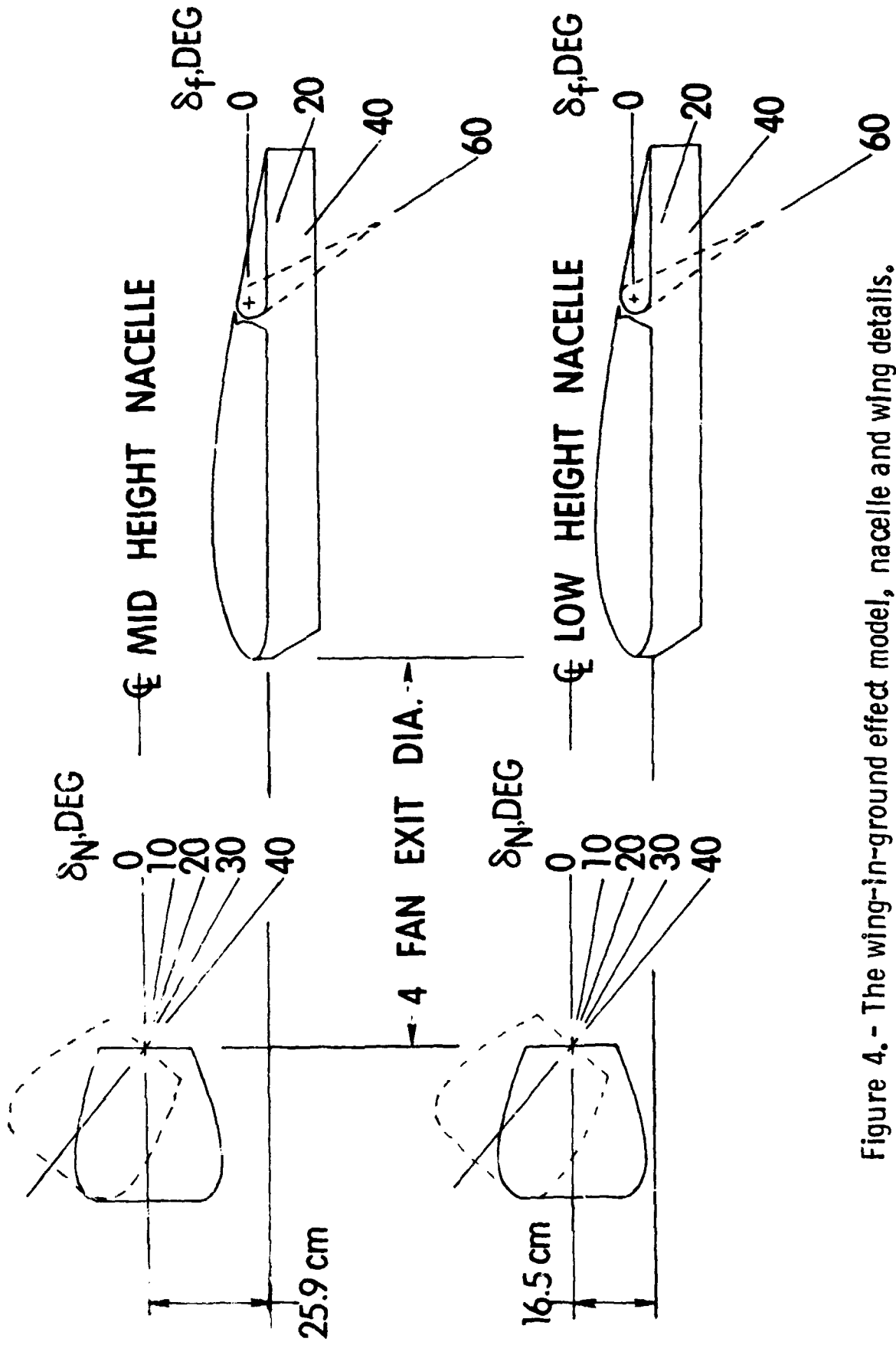


Figure 4. - The wing-in-ground effect model, nacelle and wing details.



(a) Front view
Figure 5 - Wing-in-ground effect model mounted over moving-belt groundplane
in the VSTOL tunnel

ORIGINAL PAGE IS
OF POOR QUALITY



(b) Rear view

ORIGINAL PAGE IS
OF POOR QUALITY

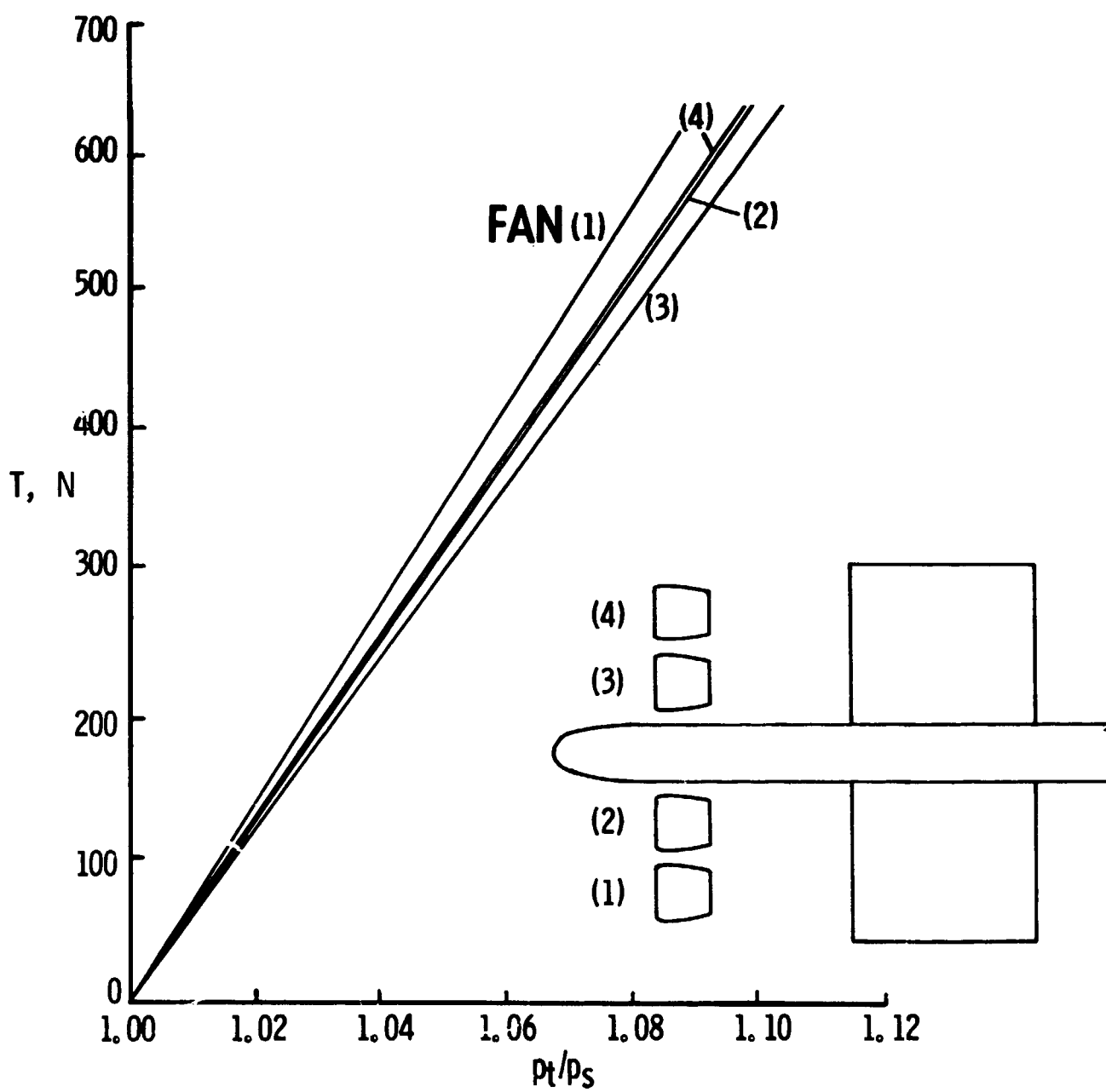


Figure 6.- Fan thrust calibration.

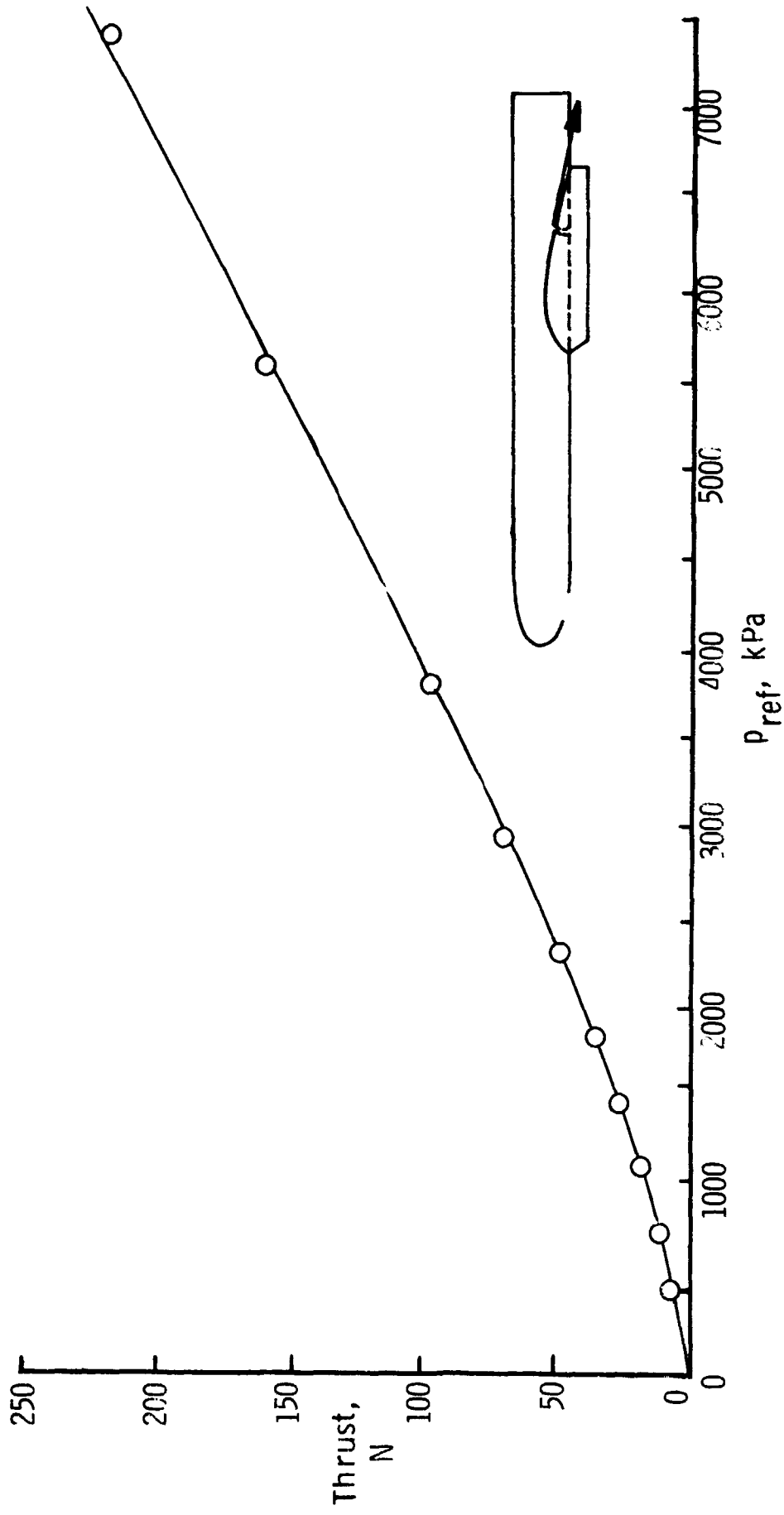


Figure 7.- The thrust calibration of the flap boundary-layer control (BLC).

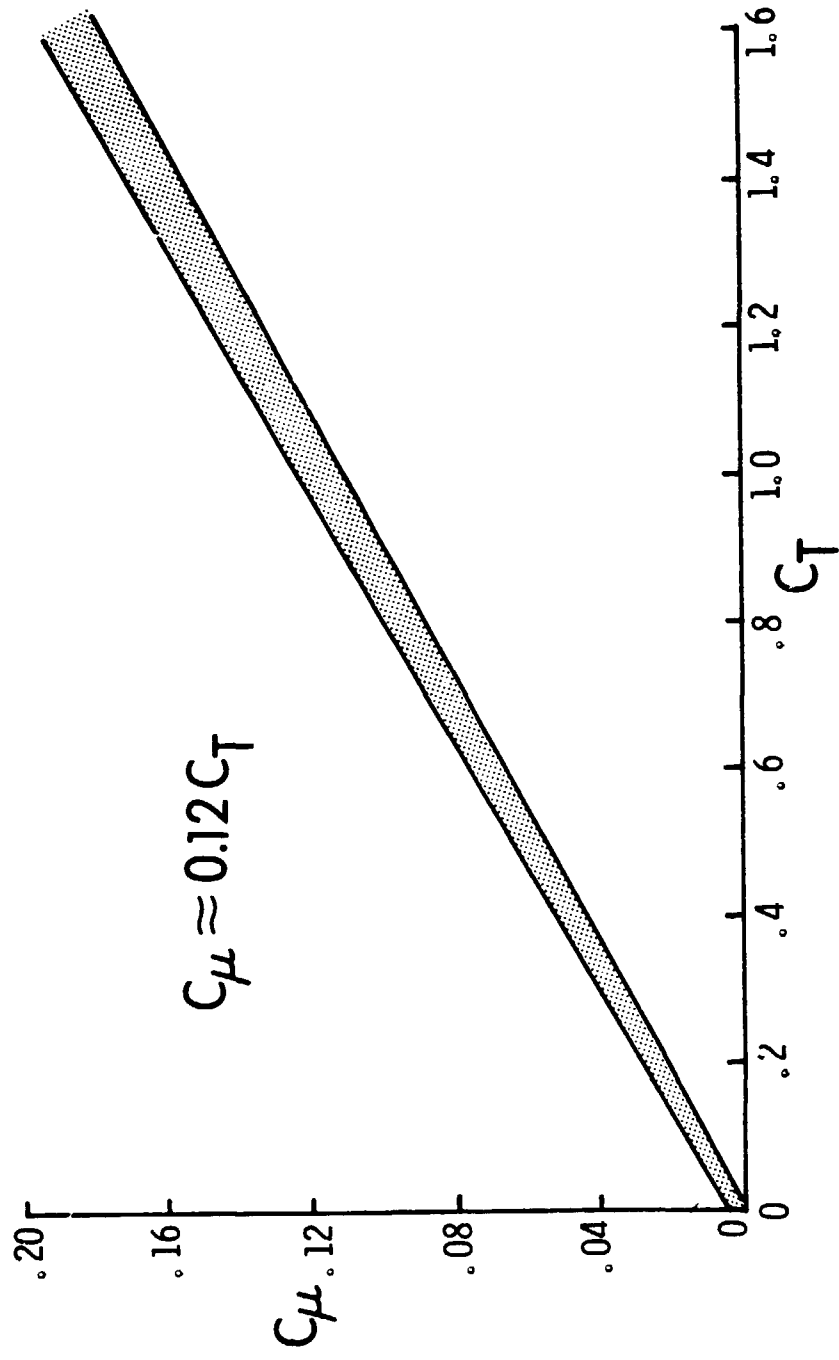


Figure 8.- The variation of C_μ with C_T

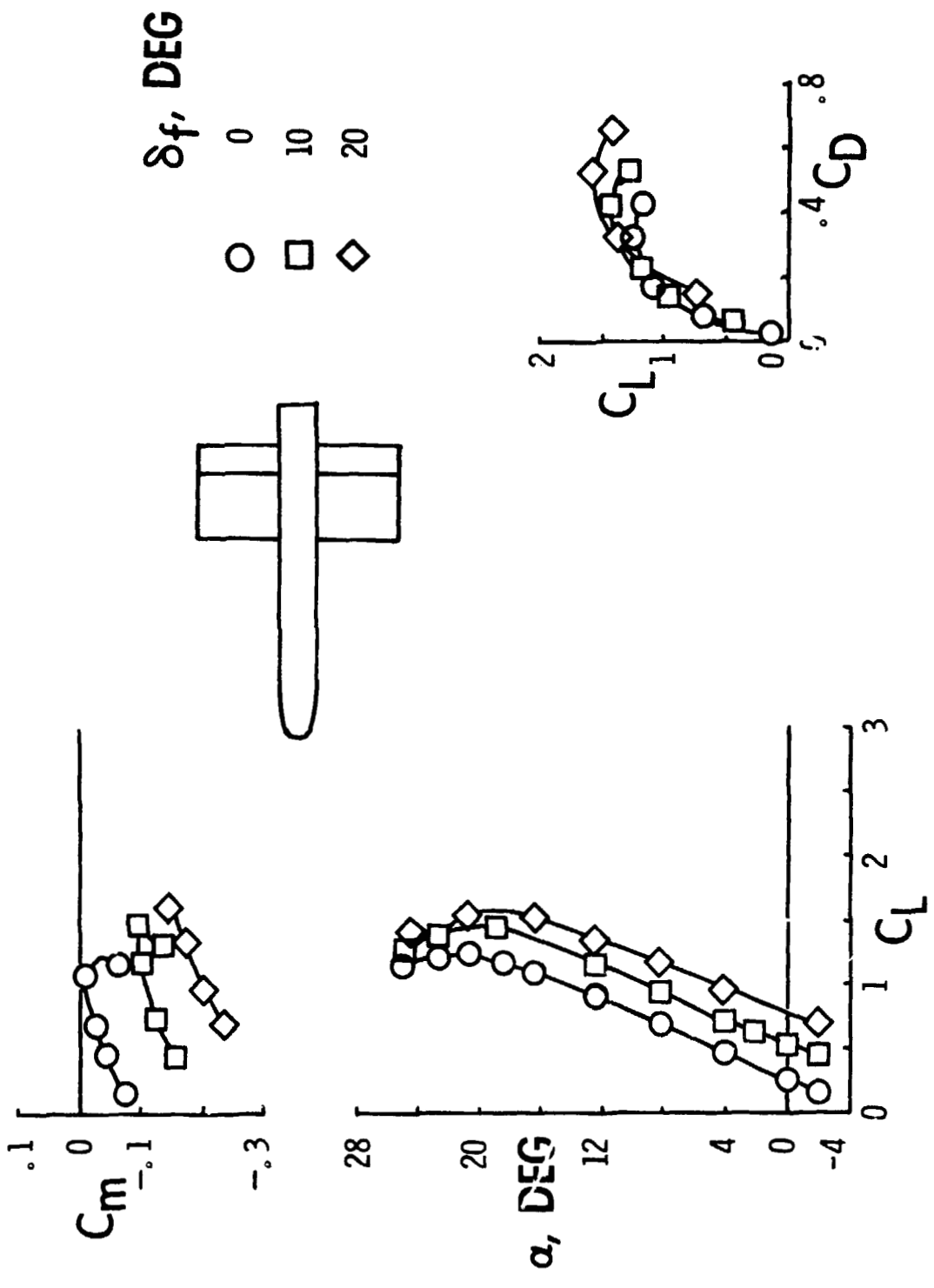
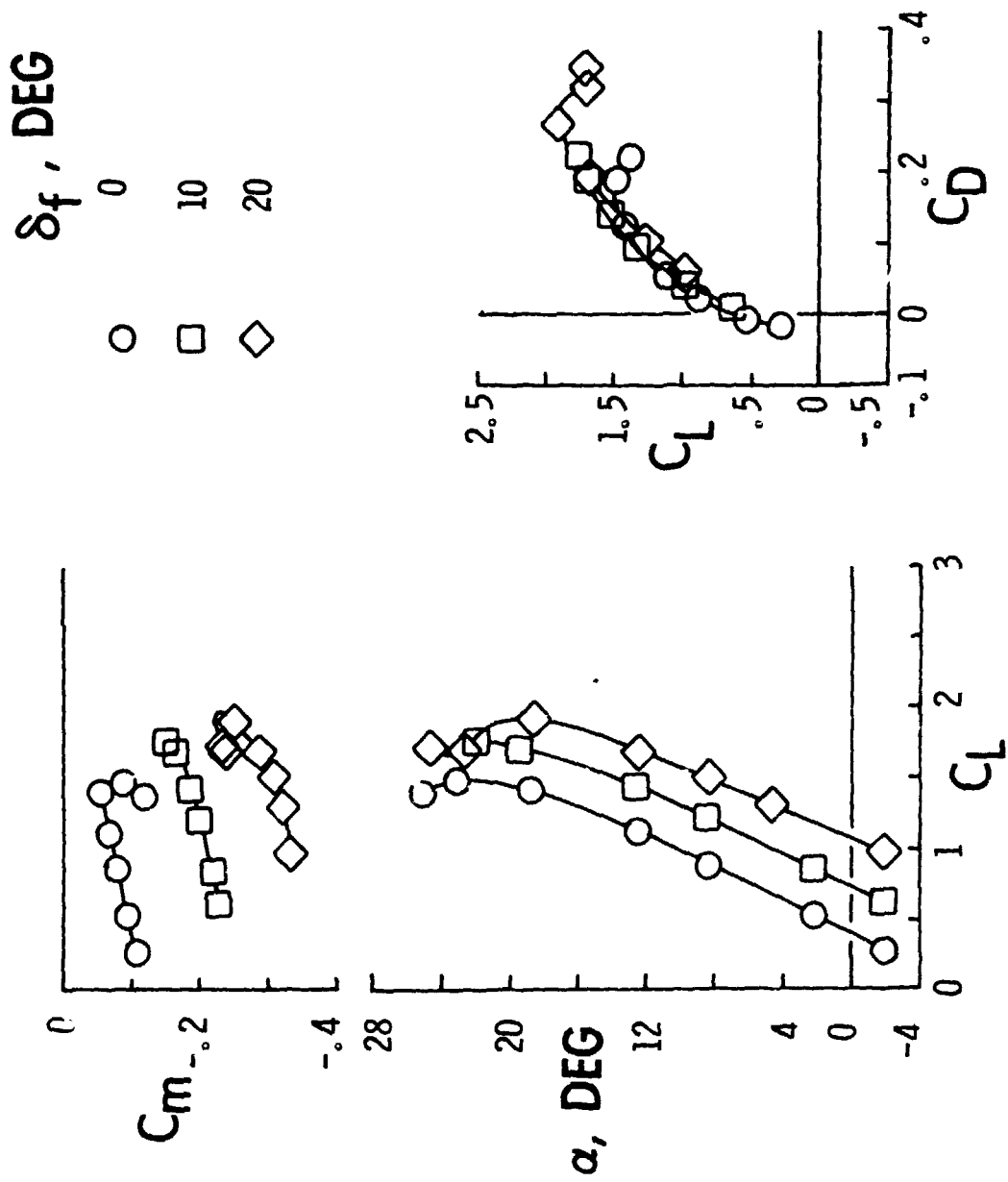


Figure 9.- The effect of flap deflection on the longitudinal aerodynamics of the wing-fuselage, $C_{\mu} = 0$



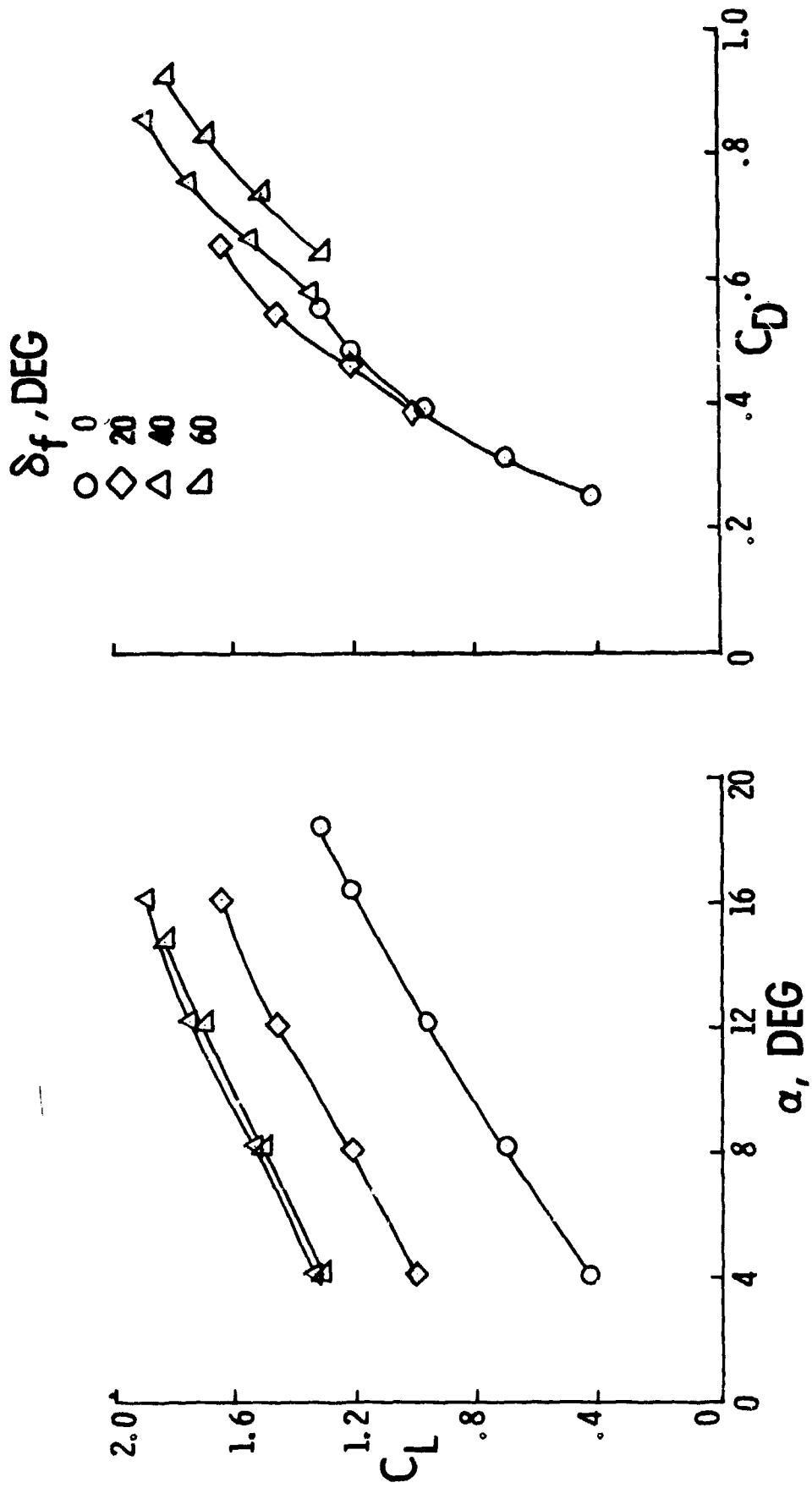


Figure 11.- The effect of flap deflection on the longitudinal aerodynamics of the complete configuration, $C_T = C_{\mu} = 0$, $\delta_N = 40^\circ$.

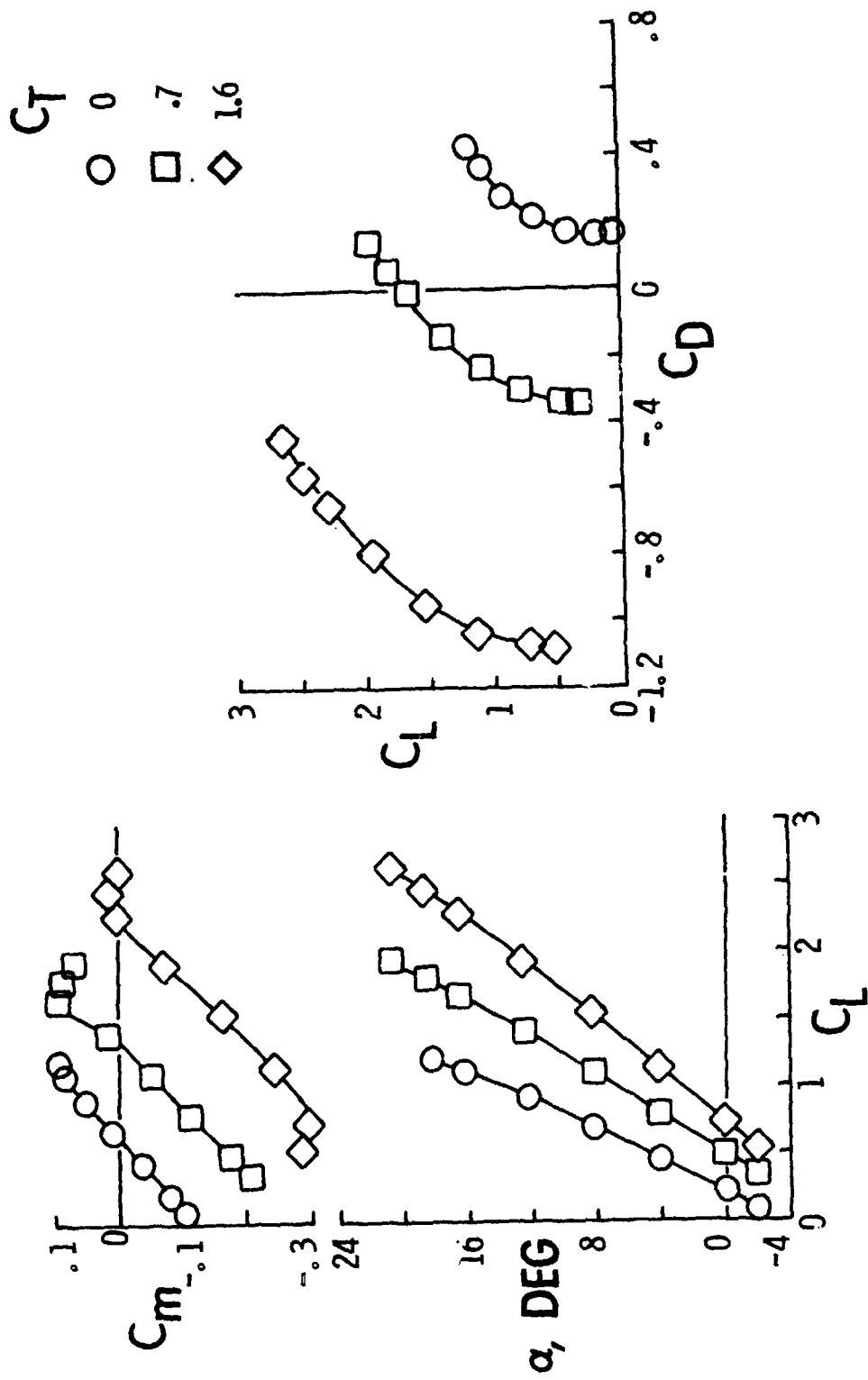


Figure 12. - The effect of thrust on the longitudinal aerodynamics of the complete configuration, $\delta_f = \delta_N = 0^\circ$, $C_{\mu} = 0.12 C_T$.

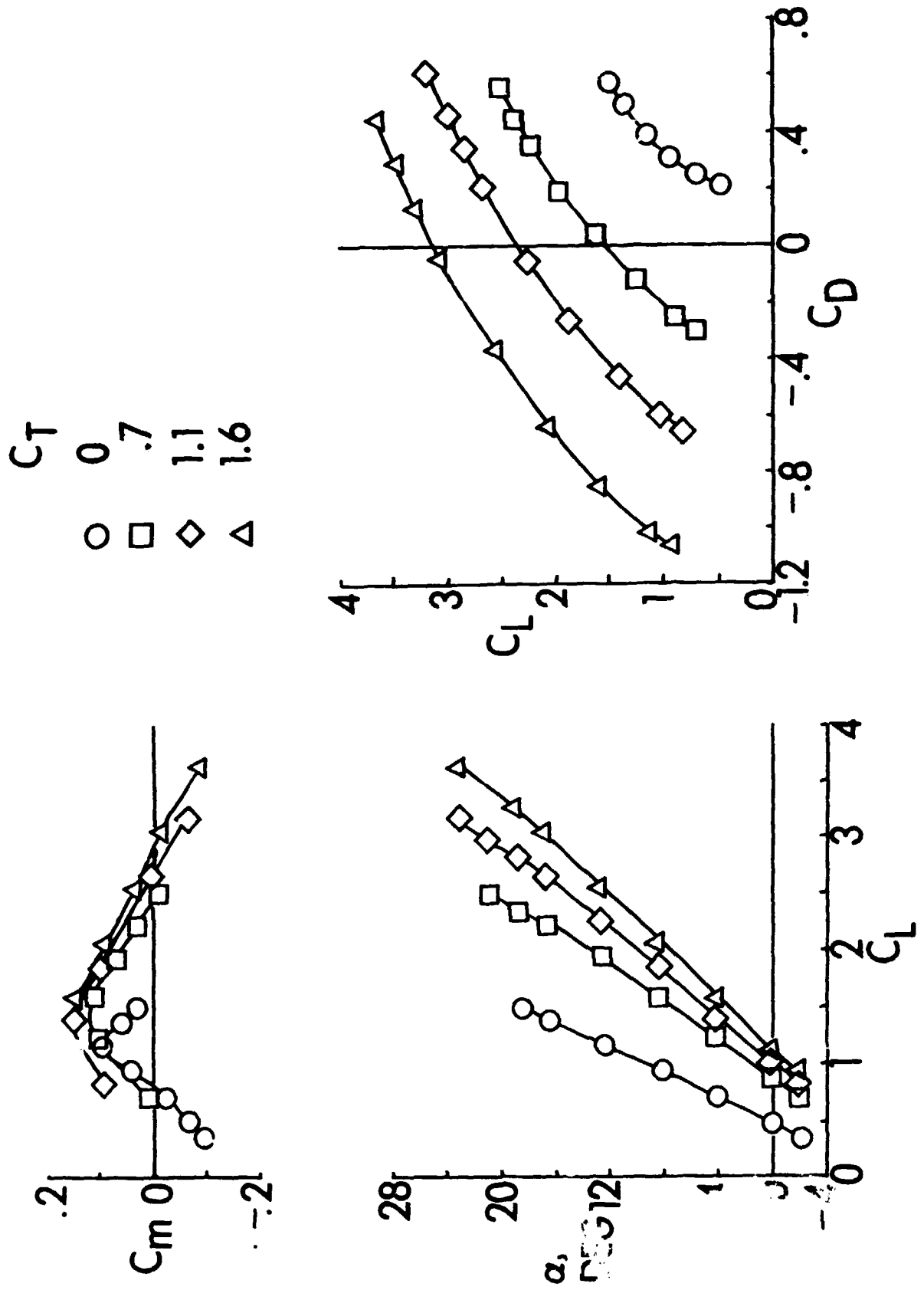


Figure 13. - The effect of thrust on the longitudinal aerodynamics of the complete configuration, $\delta_f = 10^\circ$, $\delta_N = 19^\circ$, $C_\mu = 0.12$ C_T .

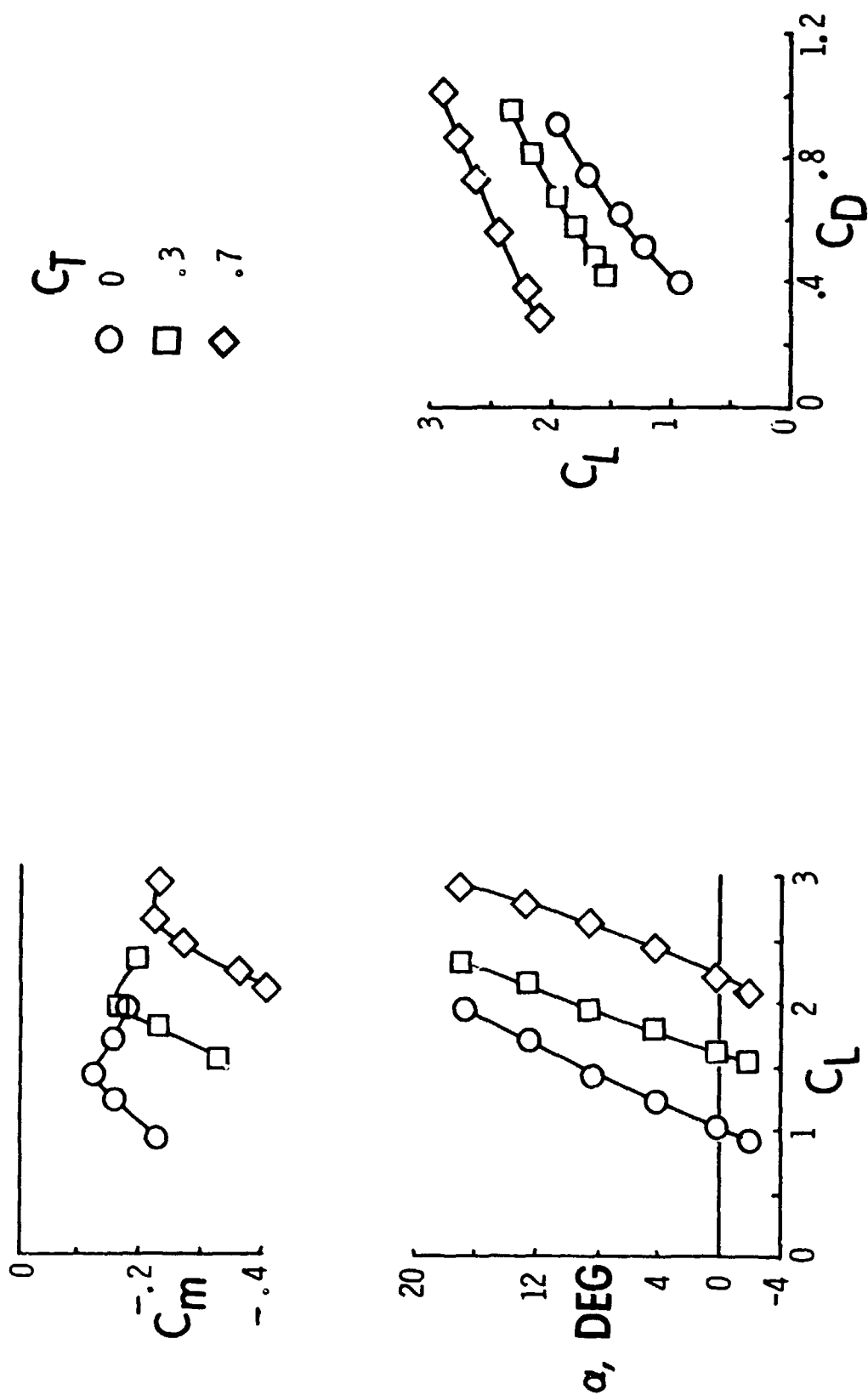


Figure 14. - The effect of thrust on the longitudinal aerodynamics of the complete configuration, $\delta_f = 40^\circ$, $\delta_N = 19^\circ$, $C_\mu = 0.12 C_T$.

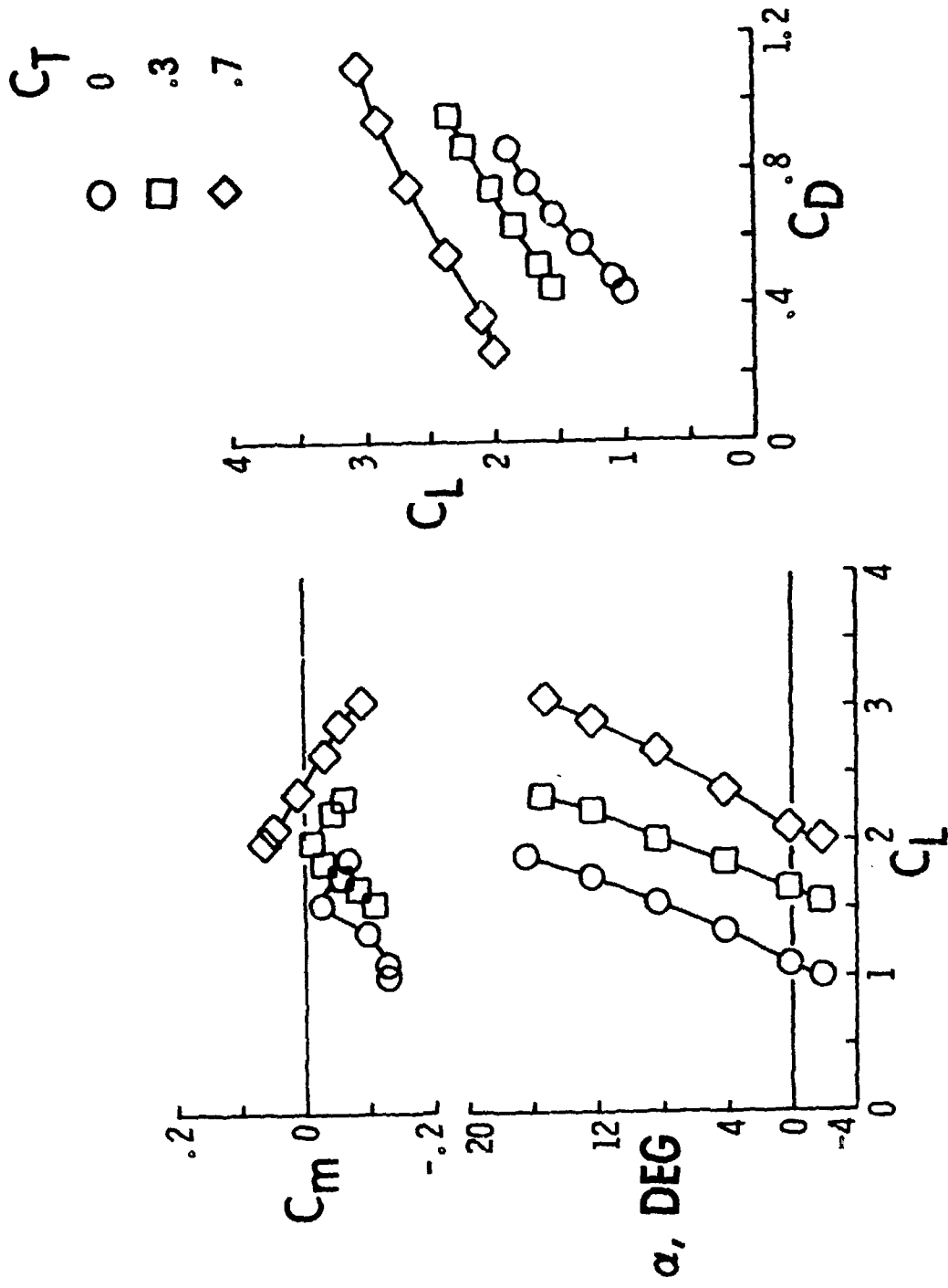


Figure 15.- The effect of thrust on the longitudinal aerodynamics of the complete configuration, $\delta_f = \delta_N = 40^\circ$, $C_{\mu} = 0.12 C_T$.

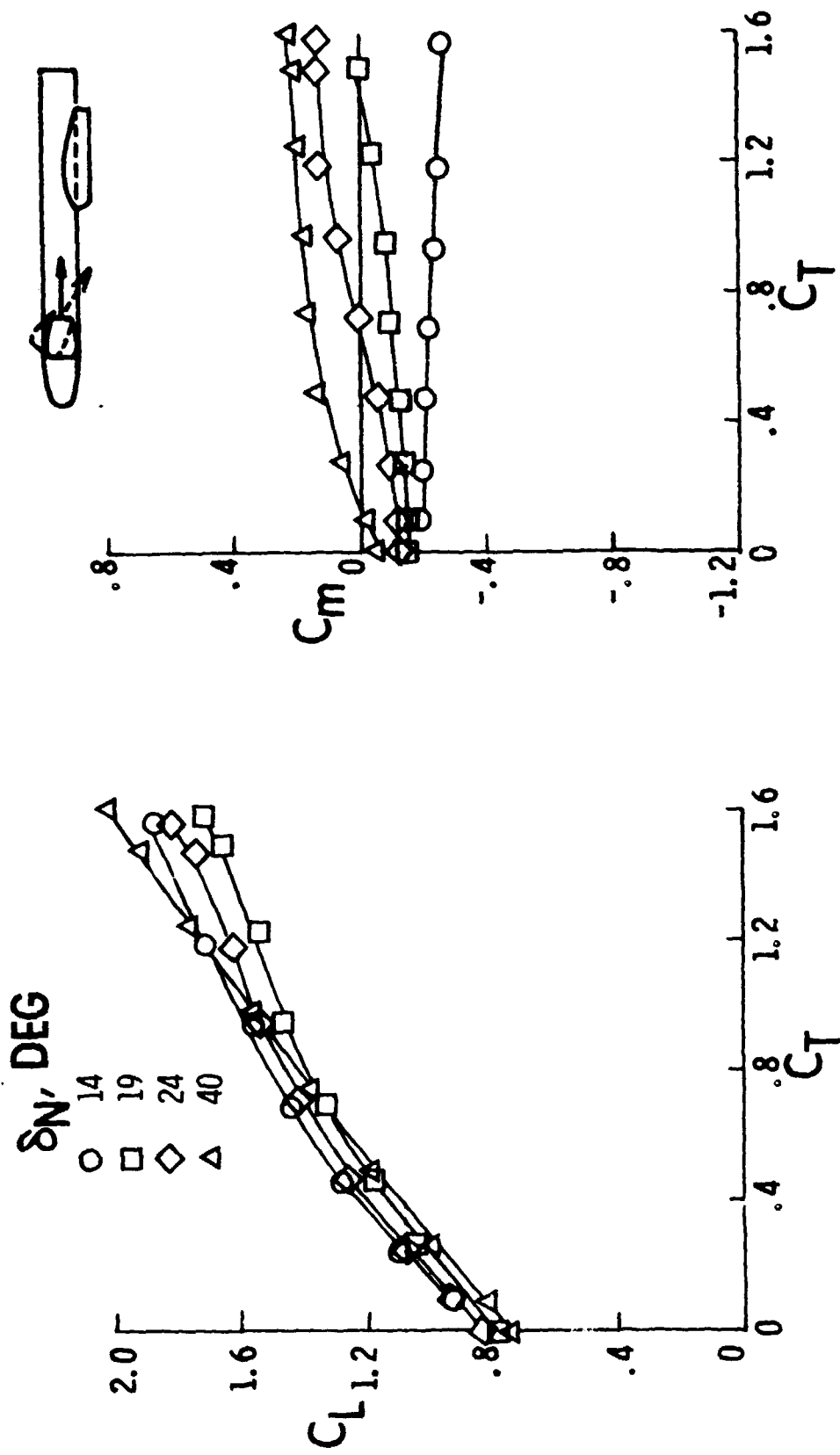


Figure 16. - The effect of deflecting fan thrust on C_L and C_m , $\alpha = 0^\circ$, $\delta_f = 20^\circ$, $C_{\mu} = 0.12 C_T$.

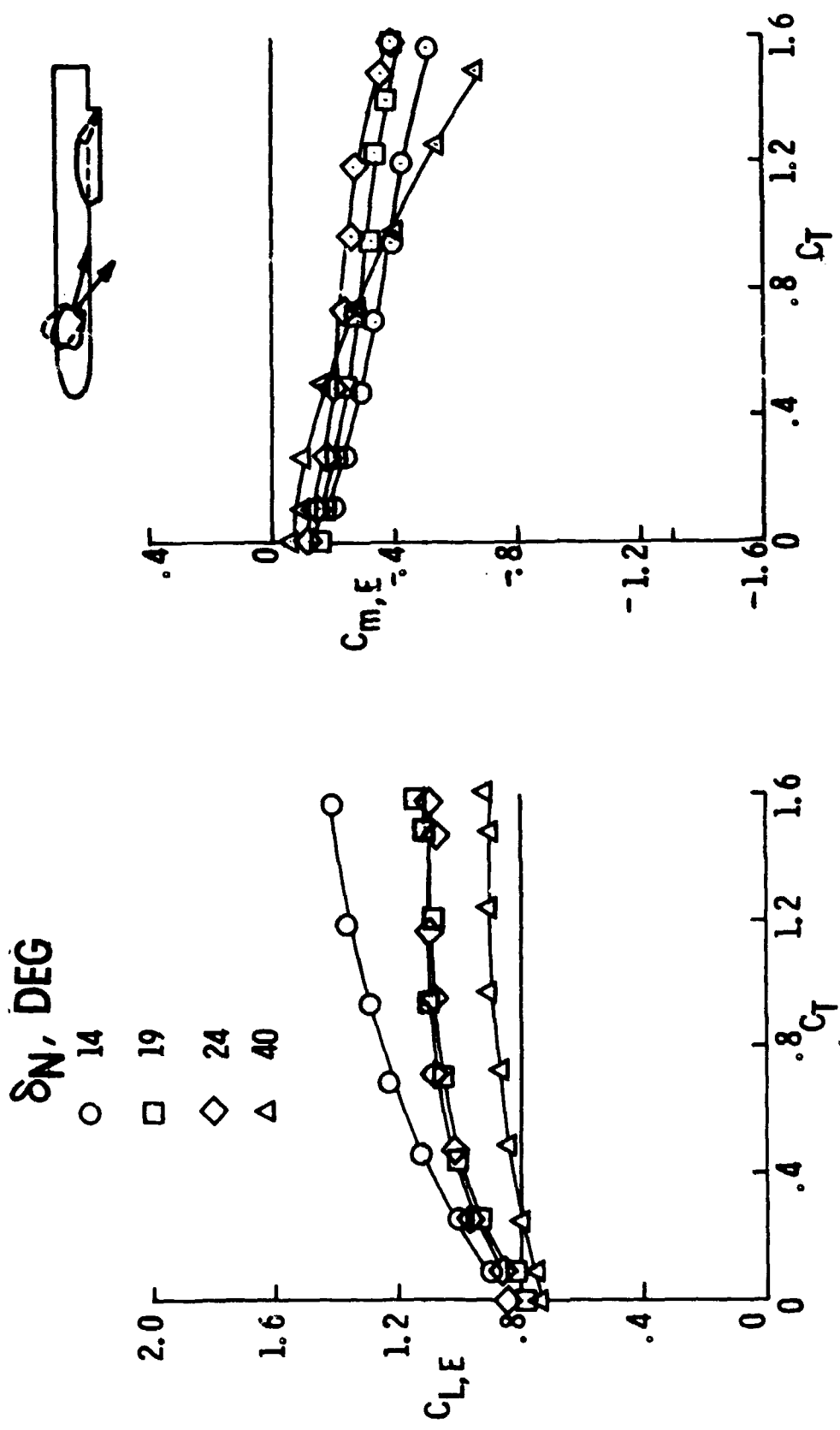


Figure 17. - The effect of deflecting fan thrust on $C_{L,E}$ and $C_{m,E}$, $\alpha = 0^\circ$, $\delta_f = 20^\circ$.

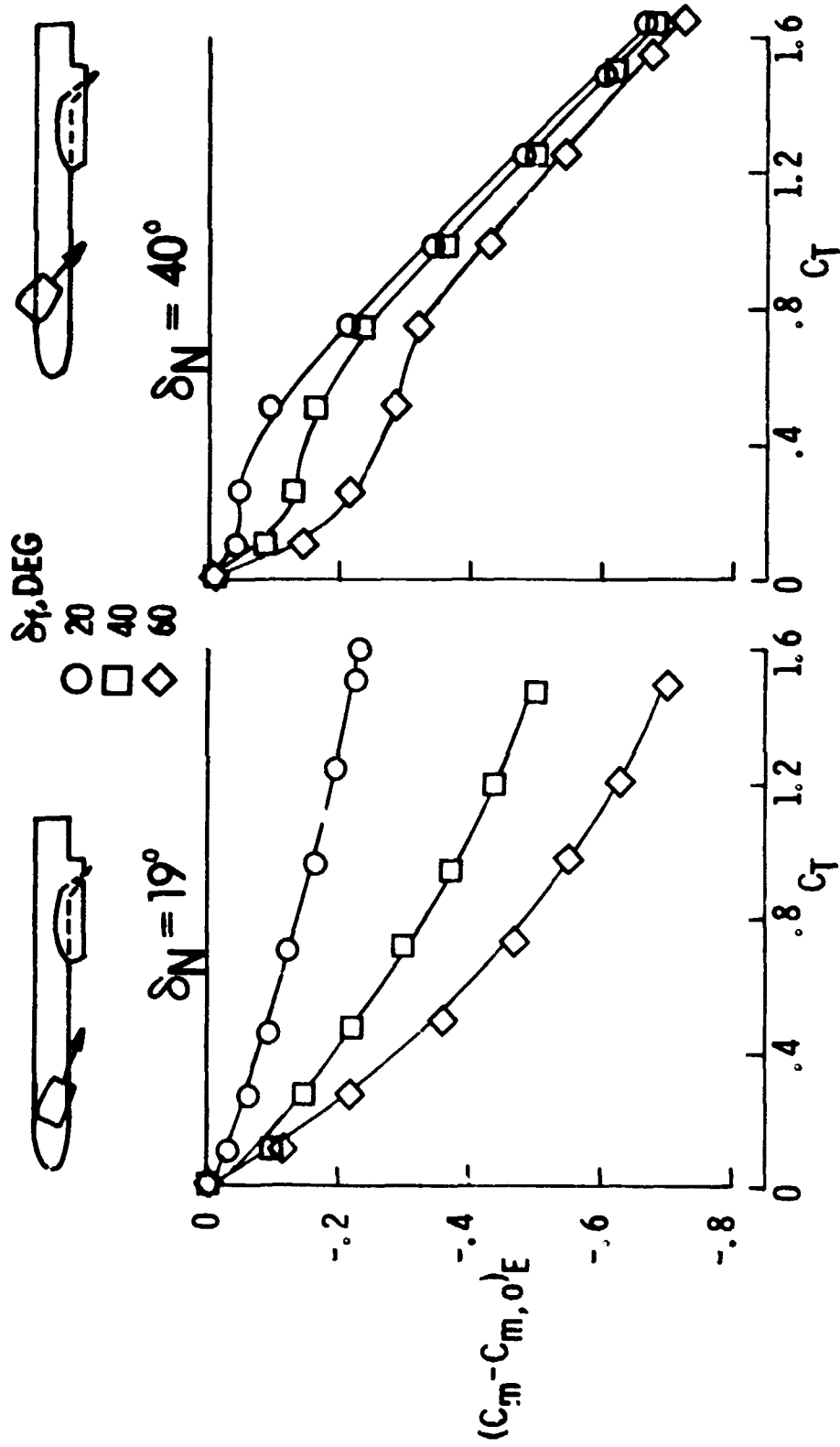


Figure 18. - The effect of flap and nozzle deflection on the thrust-removed pitching-moment coefficient, $\alpha = 0^\circ$.

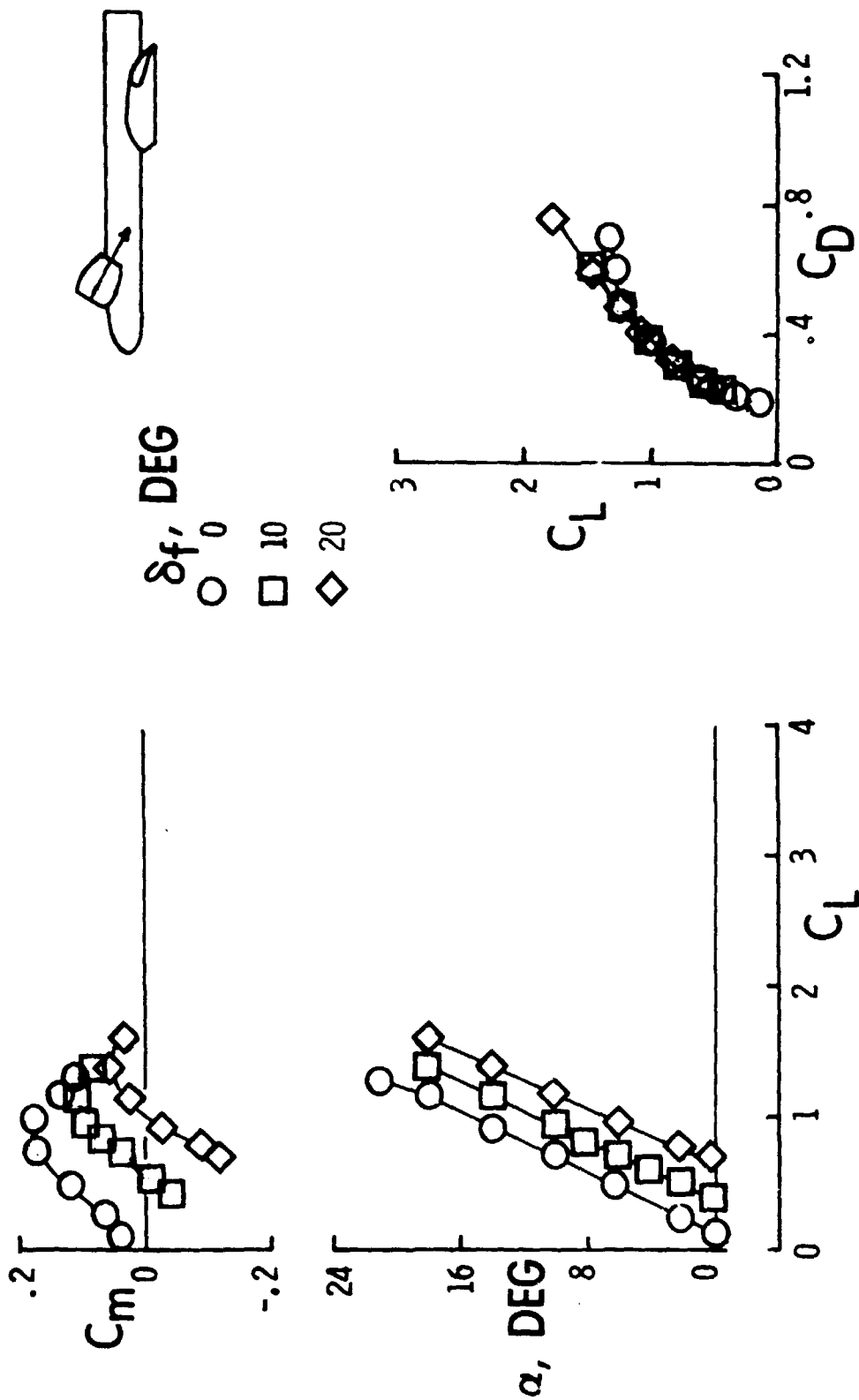


Figure 19.- The effect of flap deflection on the longitudinal aerodynamics of the complete configuration with the mid-height nacelle, $\delta_N = 26^\circ$, $C_T = 0$.

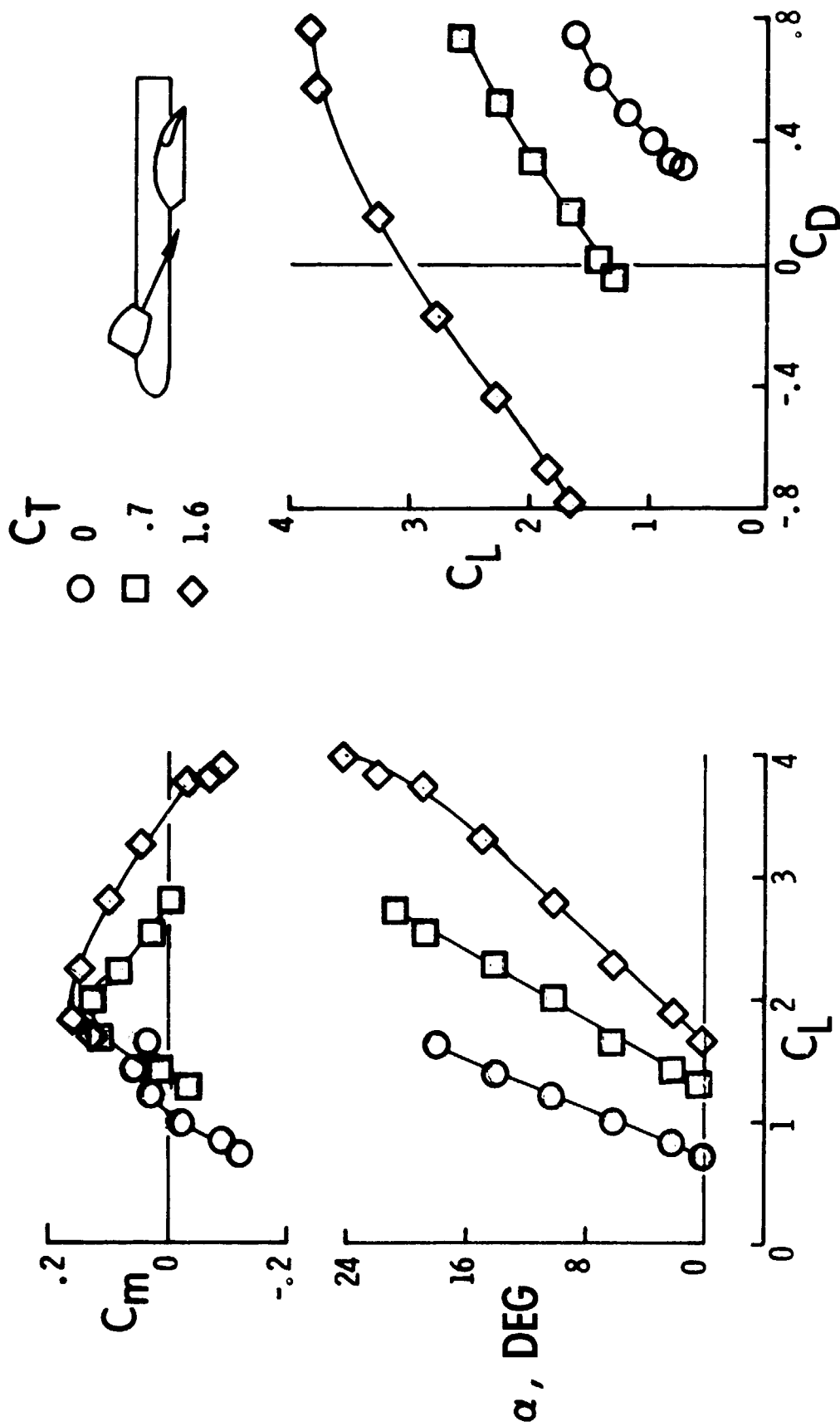


Figure 20.- The effect of thrust on the longitudinal aerodynamics of the complete configuration with the mid-height nacelle, $\delta_f = 20^\circ$, $\delta_N = 26^\circ$, $C_{\mu} = 0.12 C_T$.

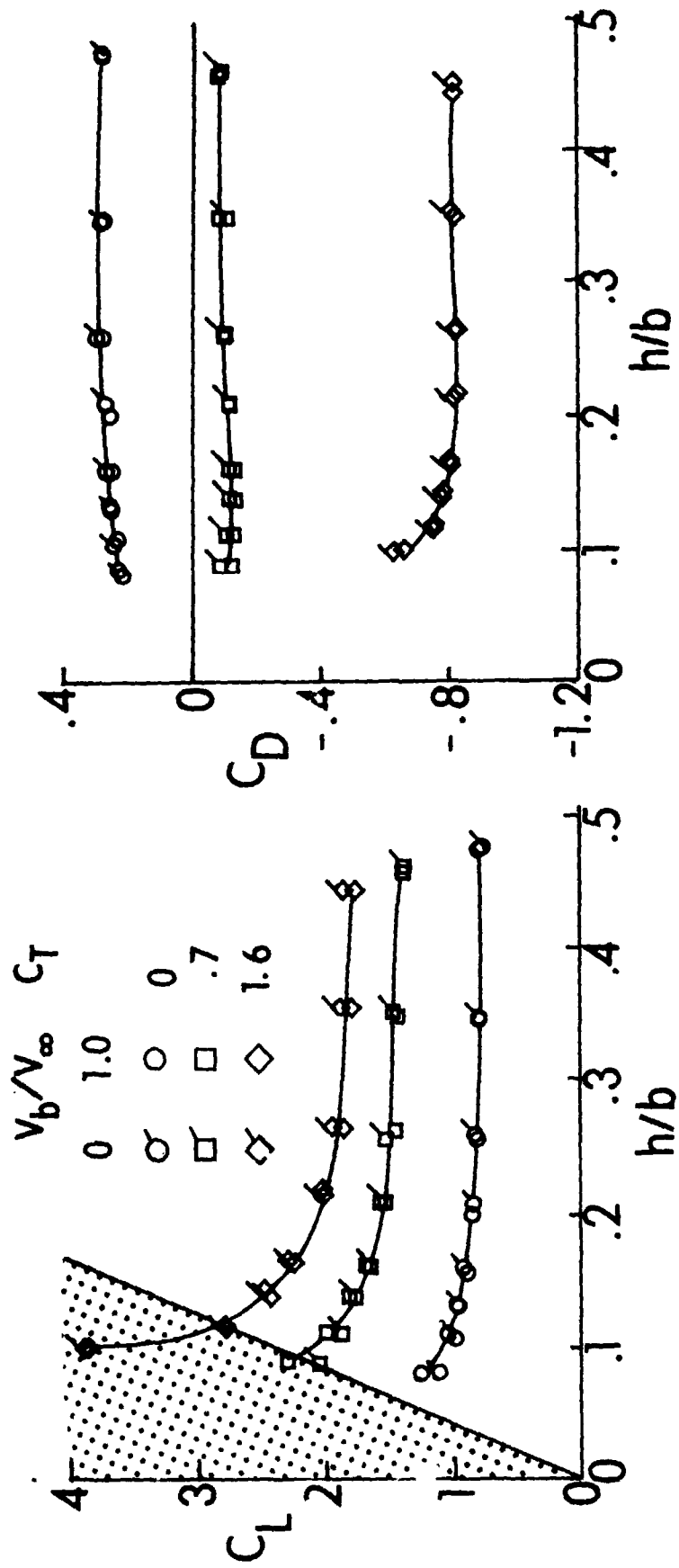


Figure 21.- The effect of the moving ground belt on the in-ground effect C_L and C_D with the boundary-layer removal compressor on, $\delta_f = 20^\circ$, $\delta_N = 24^\circ$, $\alpha = 0^\circ$.

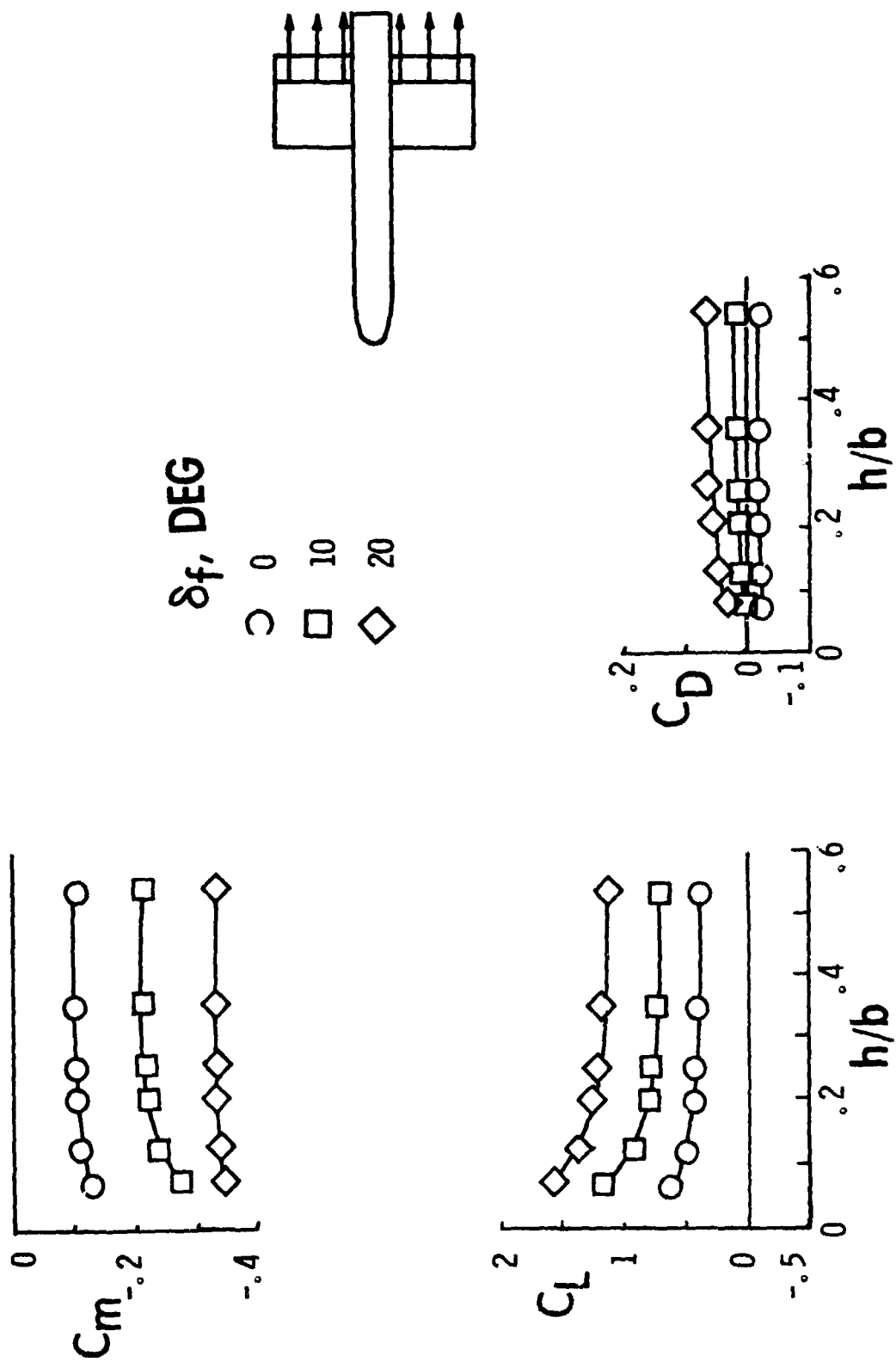


Figure 22.- The effect of flap deflection on the longitudinal aerodynamics of the wing-fuselage in-ground effect, $C_{\mu} = 0.06$, $\alpha = 0^\circ$.

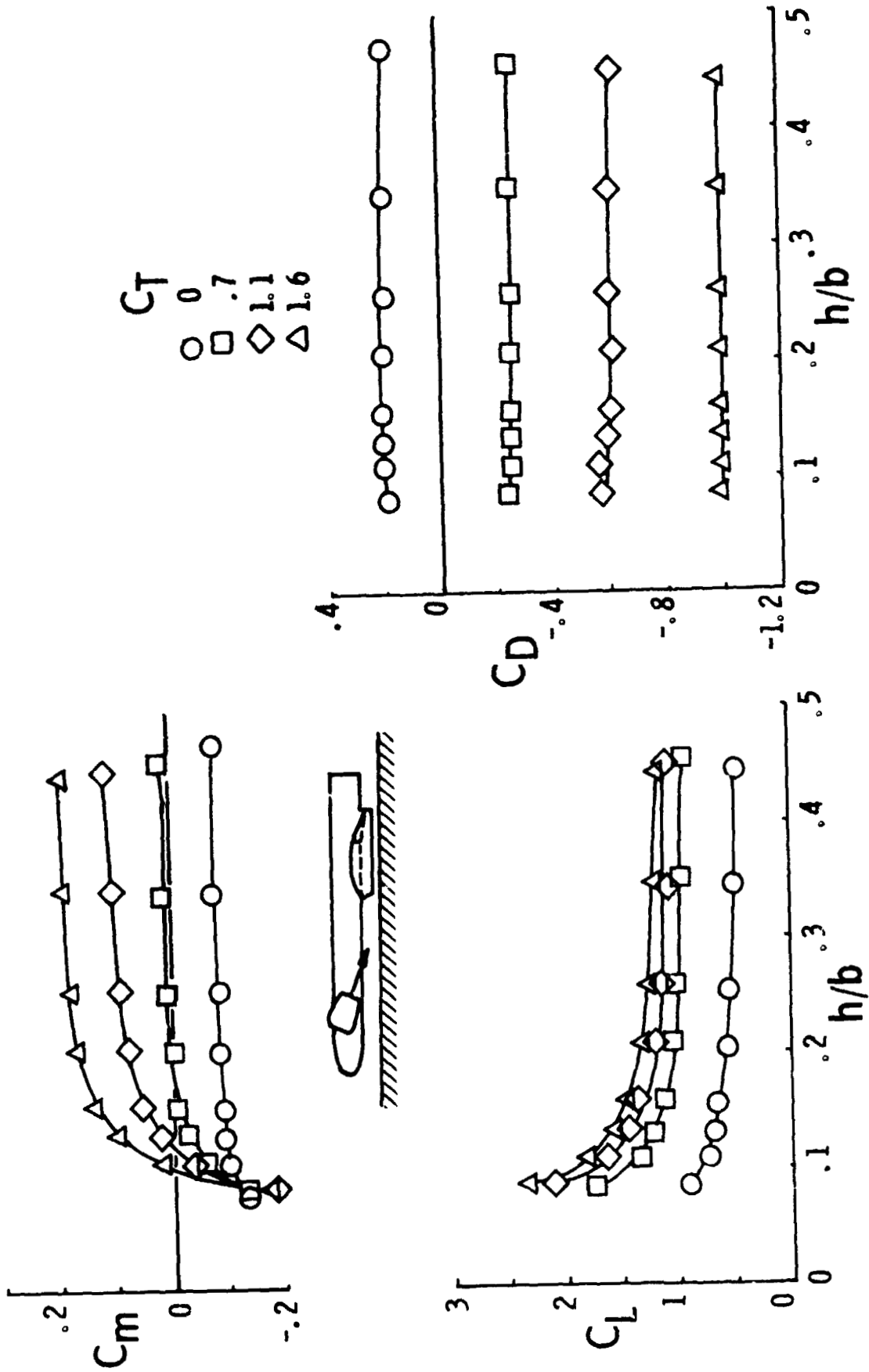


Figure 23. - The effect of thrust on the longitudinal aerodynamics of the complete configuration in-ground effect, $\delta_f = 10^\circ$, $\delta_N = 19^\circ$, $C_\mu = 0.12$, $C_T, \alpha = 0^\circ$

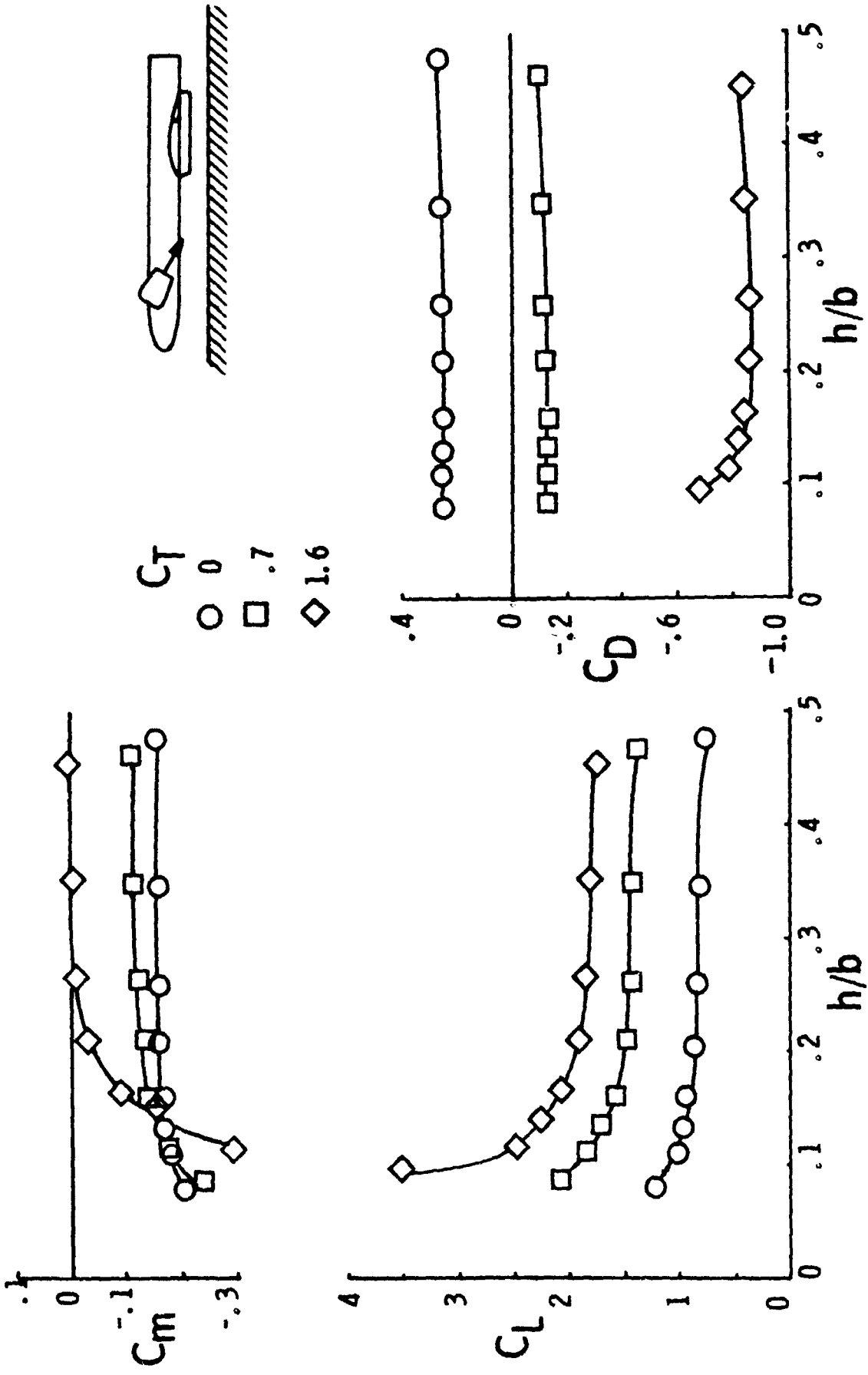


Figure 24. - The effect of thrust on the longitudinal aerodynamics of the complete configuration in-ground effect, $\delta_f = 20^\circ$, $\delta_N = 19^\circ$, $C_{\mu} = 0.12$, C_T , $\alpha = 0^\circ$.

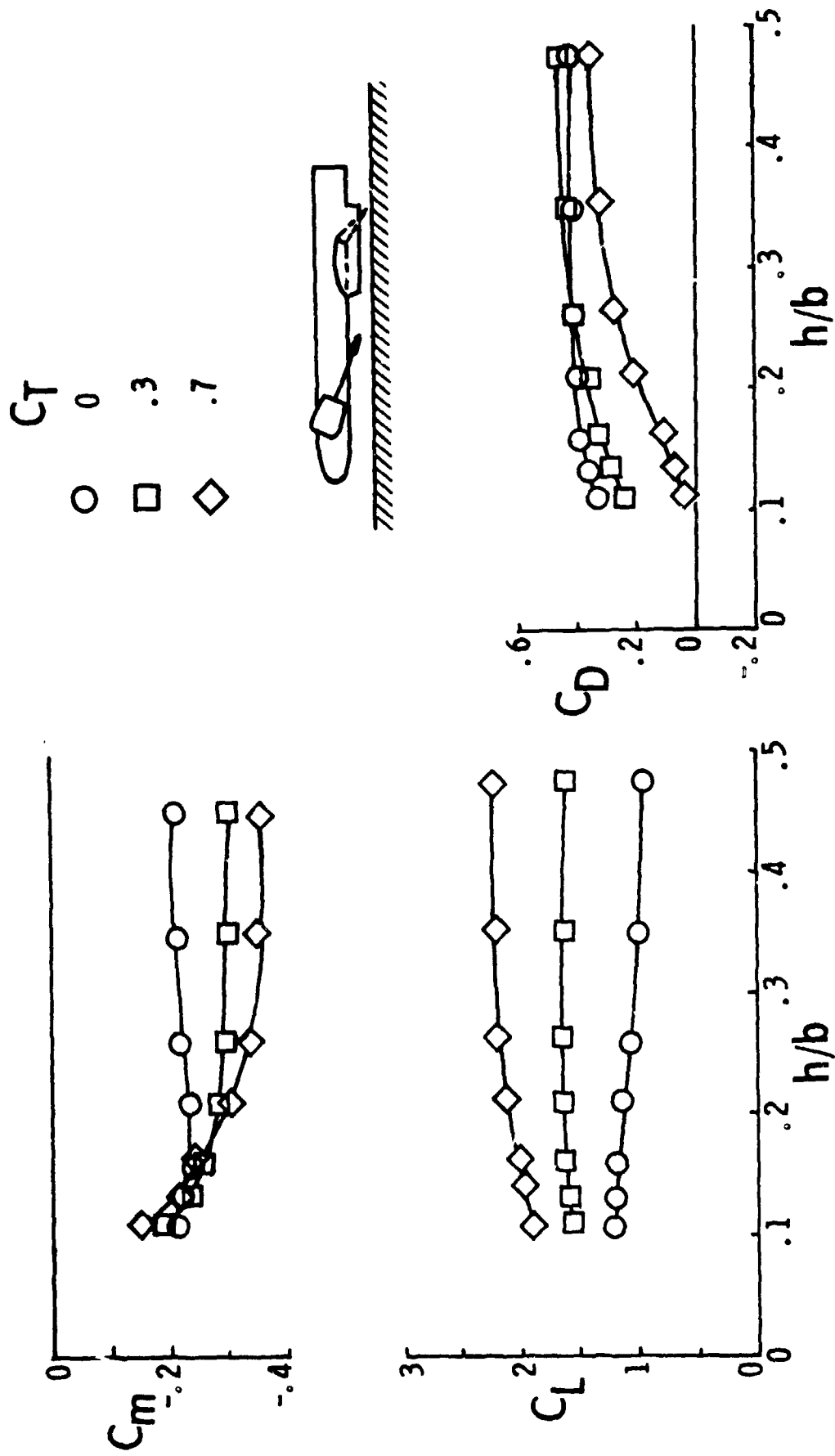


Figure 25. - The effect of thrust on the longitudinal aerodynamics of the complete configuration in-ground effect, $\delta_f = 40^\circ$, $\delta_N = 19^\circ$, $C_\mu = 0.12$, $C_T, \alpha = 0^\circ$.

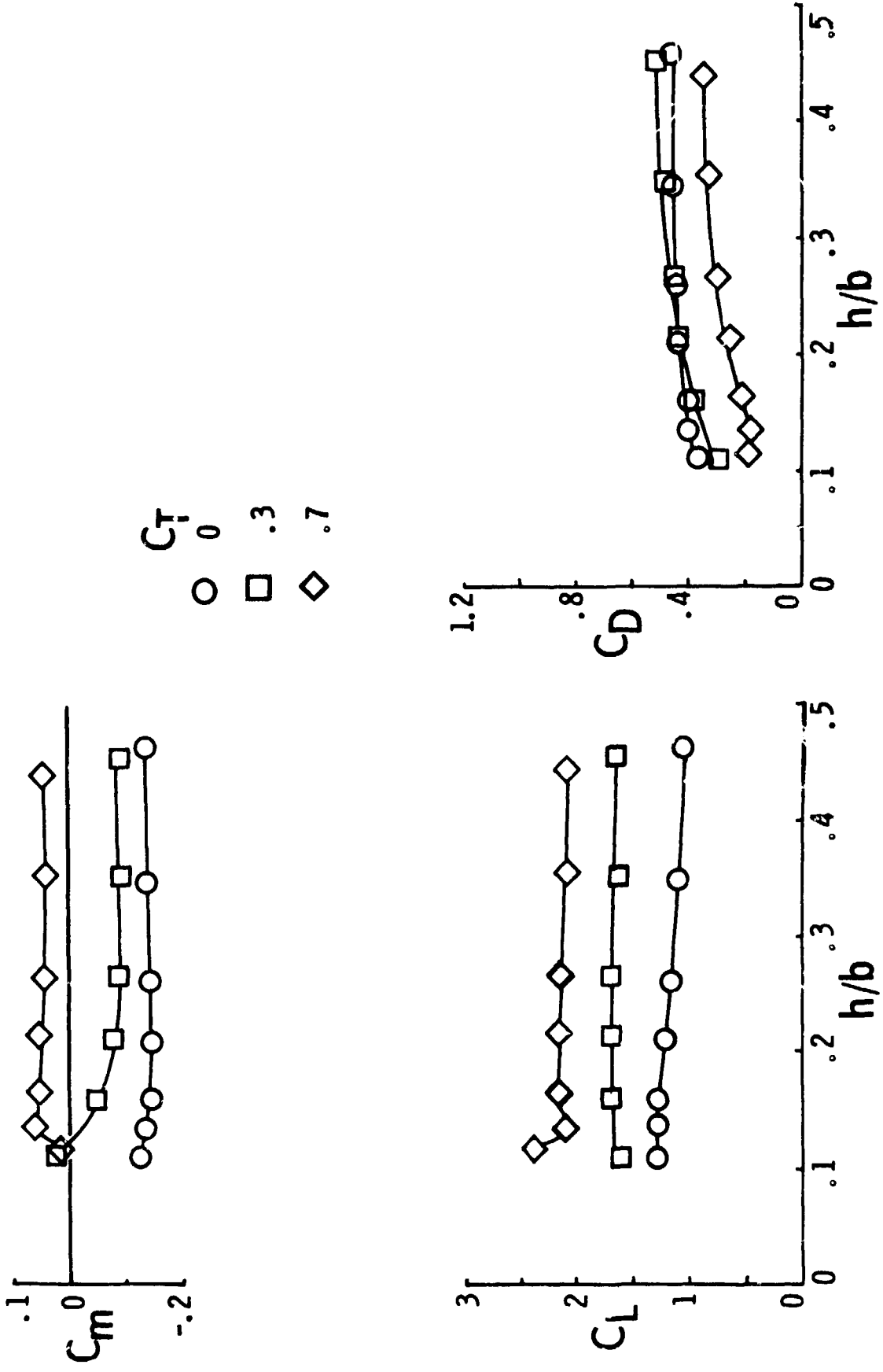


Figure 26. - The effect of thrust on the longitudinal aerodynamics of the complete configuration in-ground effect, $\delta_f = \delta_N = 40^\circ$, $C_\mu = 0.12 C_T$.

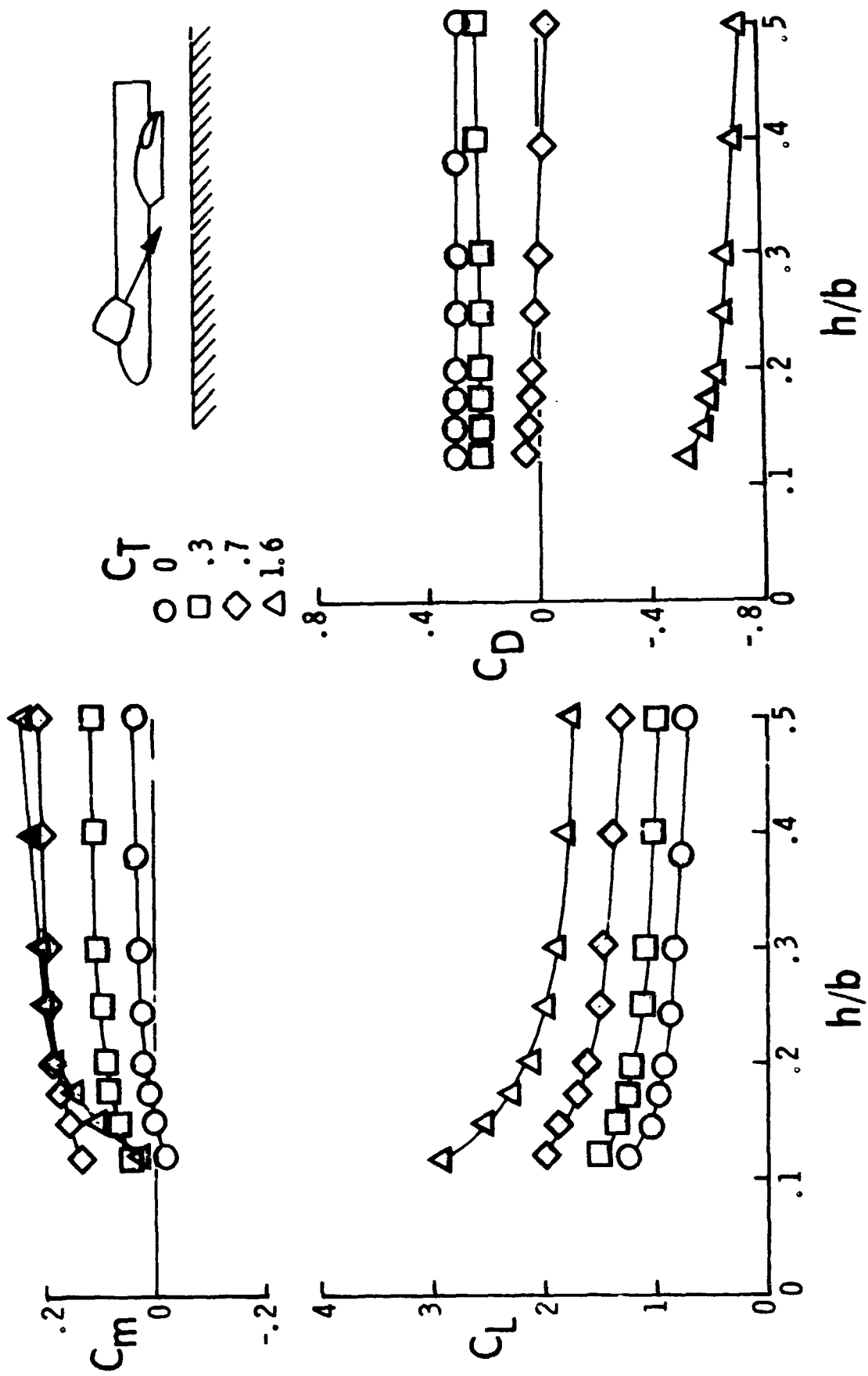


Figure 27. - The effect of thrust on the longitudinal aerodynamics of the complete configuration with the mid-height nacelle in-ground effect, $\delta_f = 10^\circ$, $\delta_N = 26^\circ$, $\alpha = 6^\circ$, $c = 0.12 C_T$.

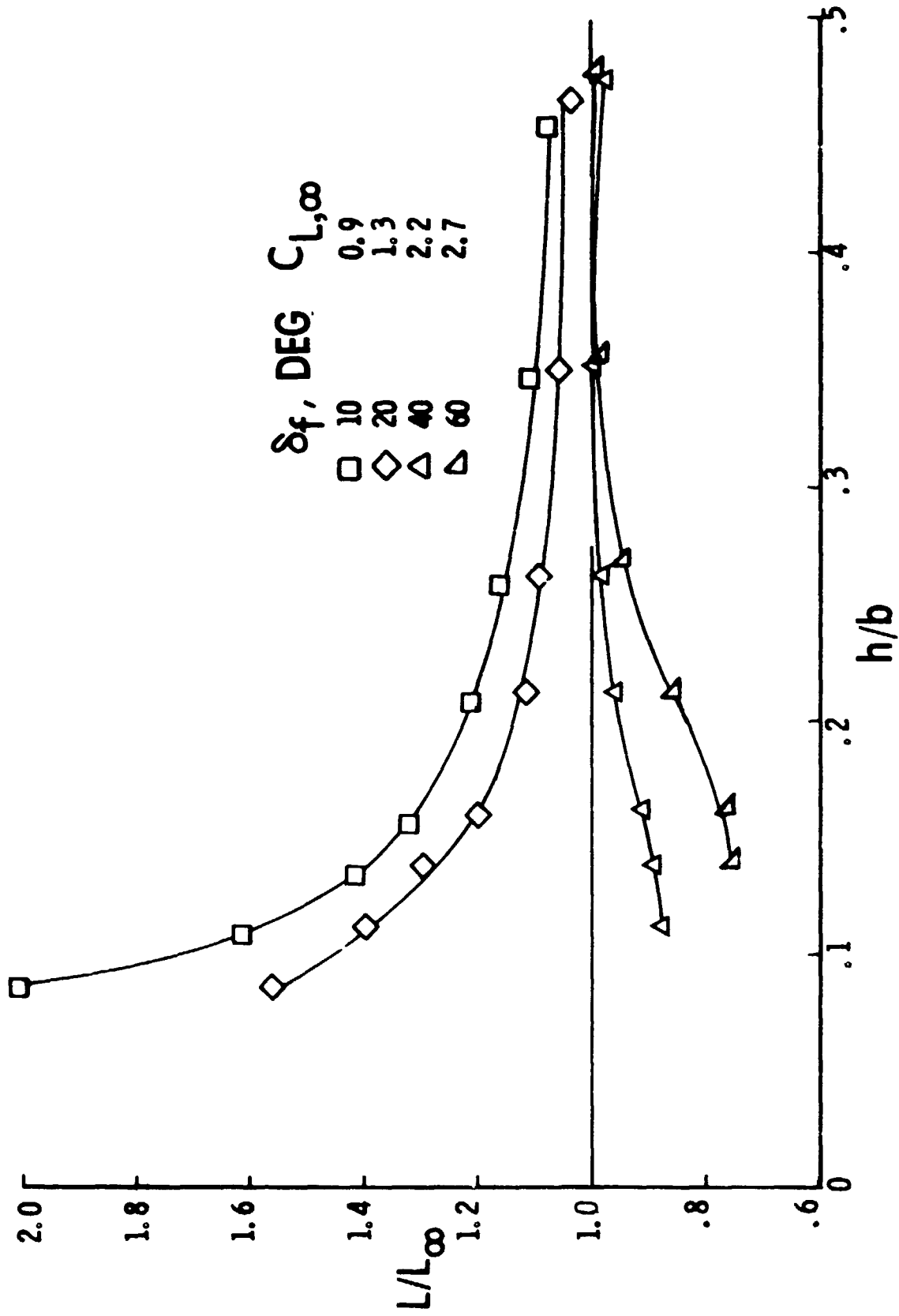
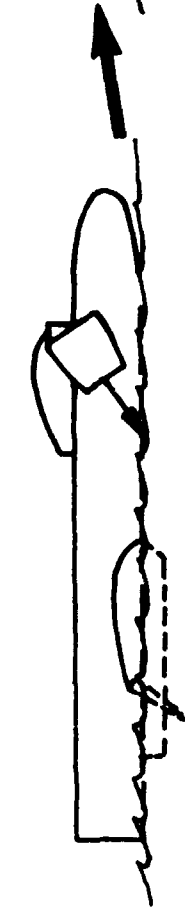


Figure 28. - The effect of flap deflection on the ratio of lift in-ground effect to lift out-of-ground effect, $\delta_N = 19^\circ$, $\alpha = 0^\circ$, $C_T = 0.7$, $C_{\mu} = 0.12 C_T$.

EXIT WATER

$V \approx 0$ kts

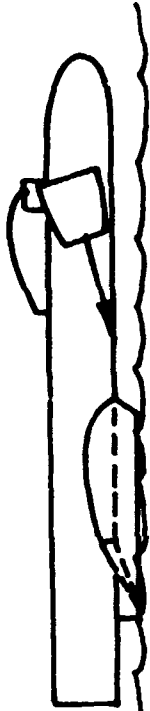
LARGE FLAP & NOZZLE DEFLECTION



ACCELERATE I.G.E. ON PAR

$0 < V < 171$ kts

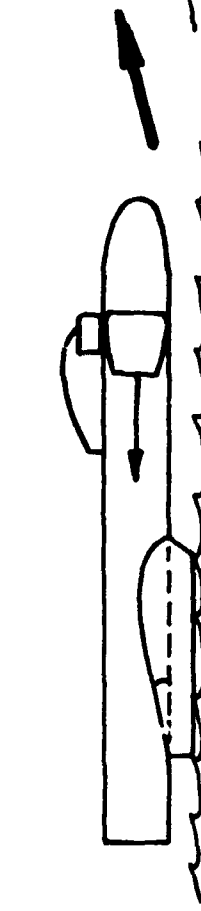
MODERATE FLAP & NOZZLE DEFLECTION



CRUISE I.G.E. OFF PAR

ZERO FLAP & NOZZLE

$171 < V < 400$ kts



CRUISE O.G.E. IF REQUIRED

ZERO FLAP & NOZZLE

$V \approx 300$ kts

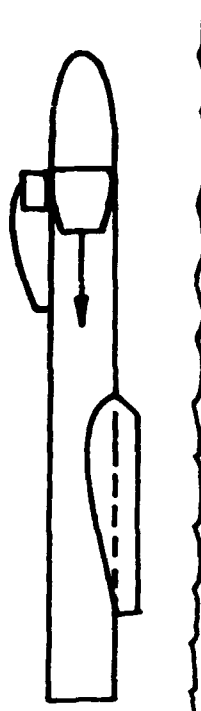


Figure 29. - A schematic of the over water takeoff operation of a wing-in-ground effect vehicle.

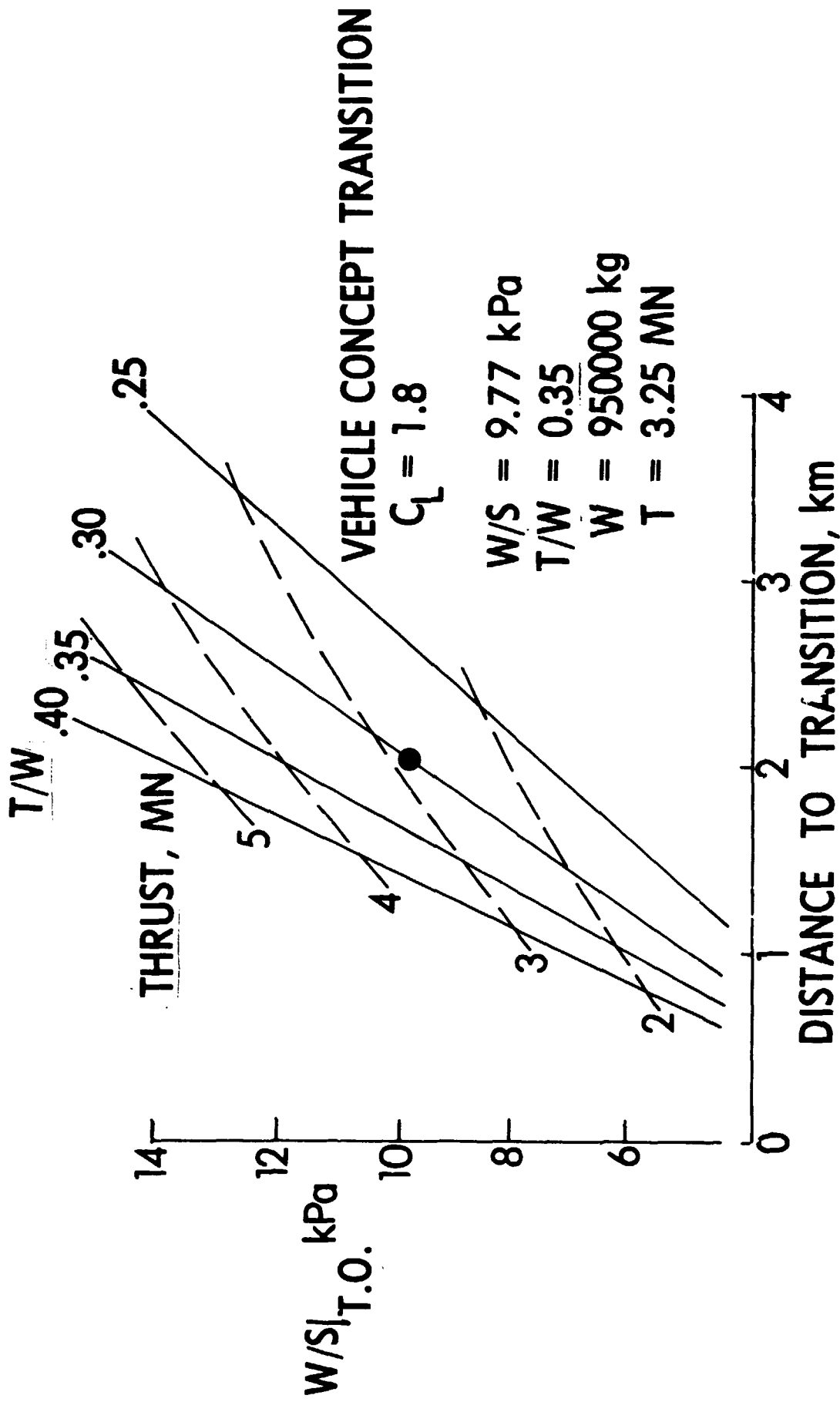


Figure 30.- The takeoff performance of a wing-in-ground effect vehicle, SI dimensions.

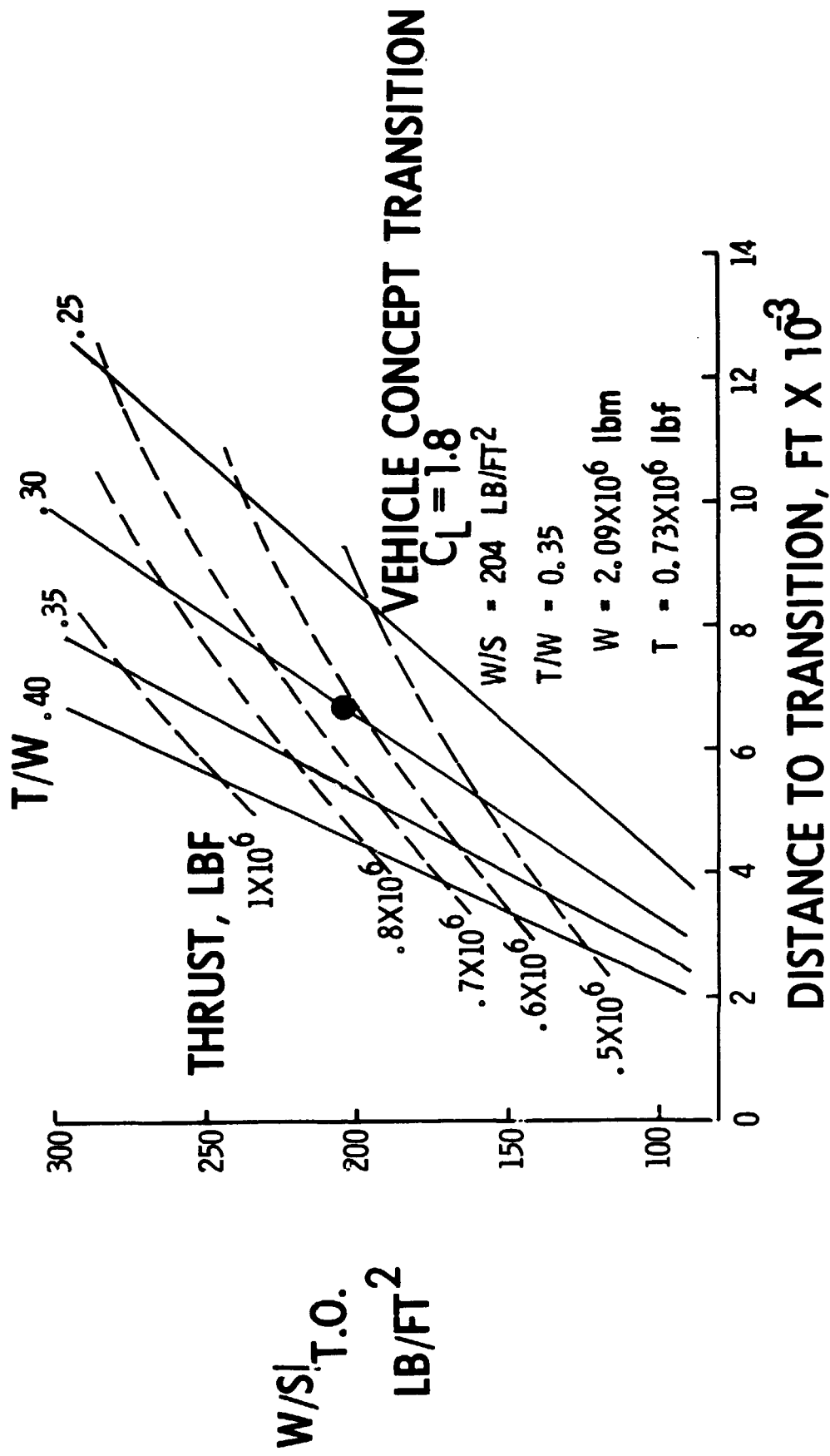


Figure 31.- The takeoff performance of a wing-in-ground effect vehicle, U.S. Customary dimensions.

APPROACH $C_L = 1.6-1.7$, THRUST = 1.0 MN
 WAVE OFF $C_L = 1.6-1.7$, THRUST = 1.2 MN

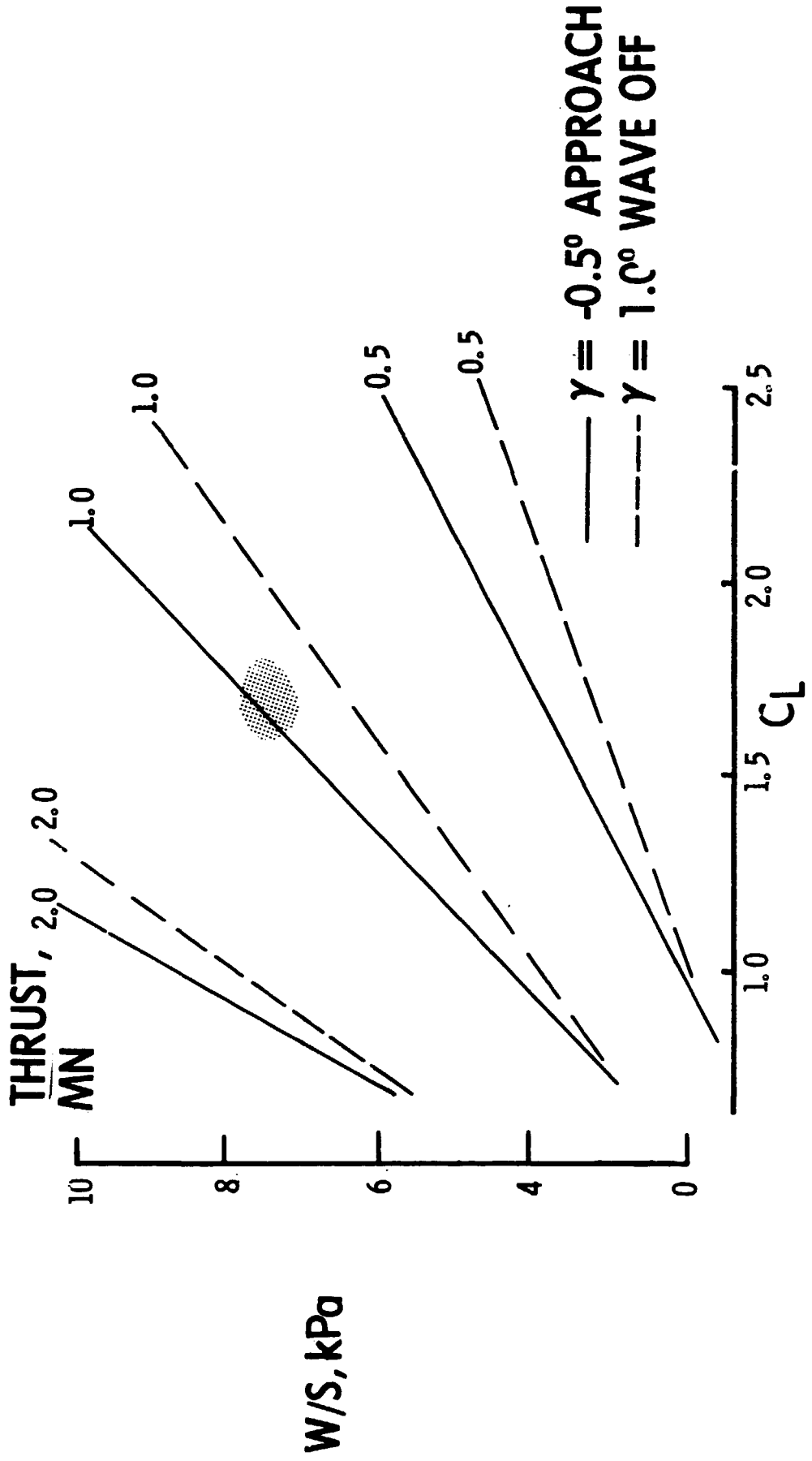


Figure 32.- The thrust required for approach and wave off, SI dimensions.

APPROACH $C_L = 1.6-1.7$, THRUST = 225,000 lbf

WAVE OFF $C_L = 1.6-1.7$, THRUST = 270,000 lbf

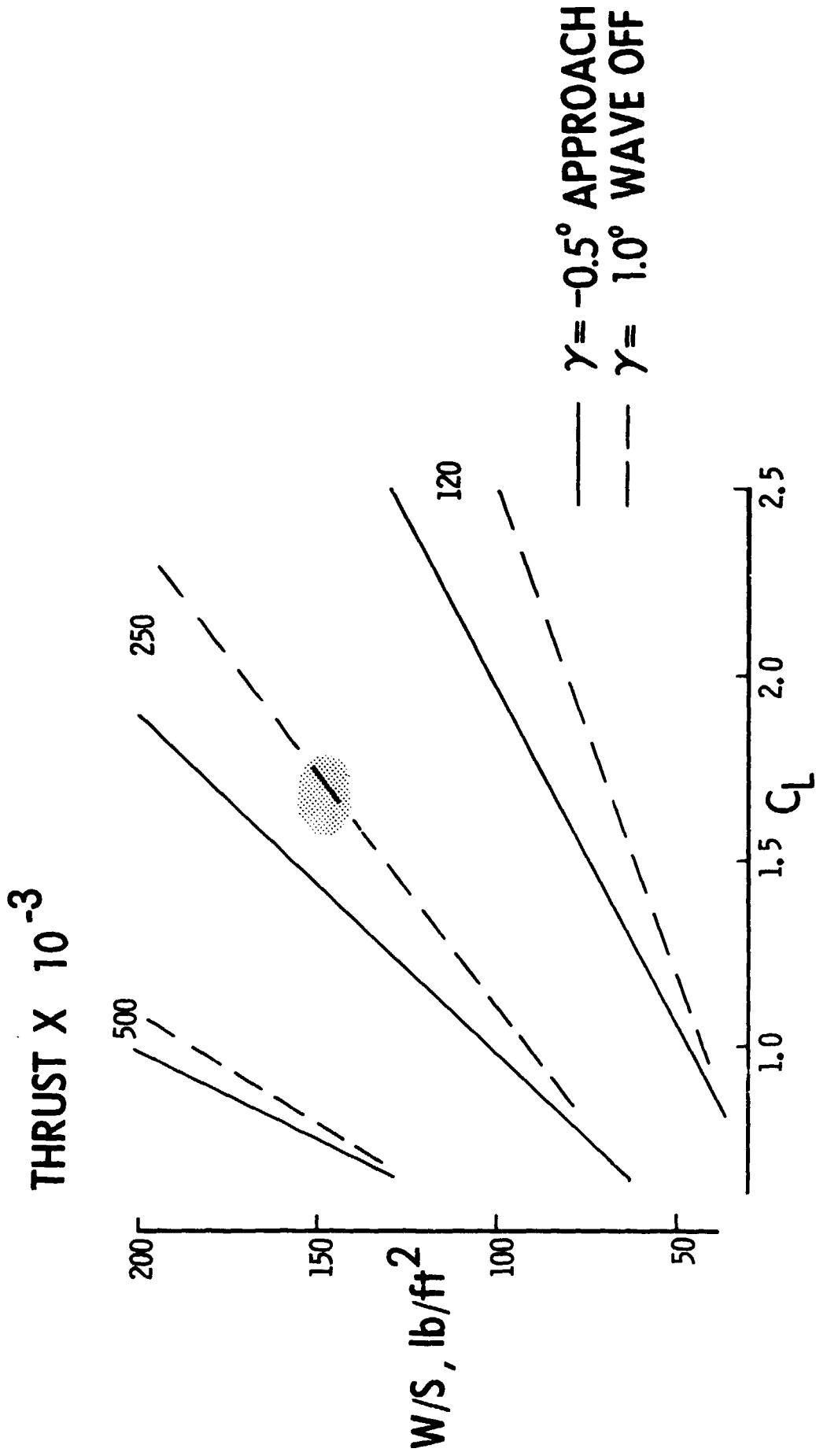


Figure 33. - The thrust required for approach and wave off, U.S. Customary Units.